VOYAGER 2 DETECTION

OF

URANIAN HECTOMETRIC RADIO ARCS

by

Allen Charles Kistler

A thesis submitted in partial fulfillment
of the requirements for the Master of
Science degree in Physics
in the Graduate College of
The University of Iowa

August 1988

Thesis supervisor: Professor Donald Gurnett

Graduate College
The University of Iowa
Iowa City, Iowa

CERTIFICATE OF APPROVAL

MASTER'S THESIS

This is to certify that the Master's thesis of

Allen Charles Kistler

has been approved by the Examining Committee for the thesis requirement for the Master of Science degree in Physics at the August 1988 graduation.

Thesis committee: Daniel A. Hunnett
Thesis supervisor

Christopher K. Gu
Member

Wynne Calvert
Member

ACKNOWLEDGEMENTS

I would like to thank a few people who have helped along the way in the production of this thesis:

Christoph Goertz for several early discussions about plasma density models and for pointing out the arc polarization should be investigated;

Larry Granroth for his program to calculate Voyager and Uranian moon ephemeris;

William Farrell and Wynne Calvert for access to their copy of the PRA data;

James Warwick for permission to use the PRA data;

Alan Tribble for a copy of his TEX file which produces a great title page; and

Donald Gurnett, most of all, for giving me an opportunity to work on this topic and for his guidance and patience in the development of this thesis.

This work was supported by NASA grant NGL-16-001-043 and JPL contract 954013.

ABSTRACT

In late January of 1986, the Voyager 2 interplanetary spacecraft made a close approach to the planet Uranus. In the region of 700 kilohertz the Planetary Radio Astronomy experiment detected periodic "radio arcs" which resemble a similar phenomenon associated with Jupiter and its moon Io. Multiple reflections of Alfvén waves generated by Jupiter's moon Io have been proposed to explain the periodic nature of the Jovian arcs. This paper proposes a similar mechanism to explain the periodic radio arcs observed near Uranus. Consideration of the three innermost large moons of Uranus shows that the second moon, Ariel, is the most likely source of Alfvén waves in the Uranian system. The analysis involves consideration of geometric constraints on the radiation and development of a simplified model of the Uranian magnetospheric plasma density.

TABLE OF CONTENTS

LIST OF TABLES

LIST OF FIGURES

CHAPTER I

INTRODUCTION

In late January of 1986, the Voyager 2 interplanetary spacecraft made a close pass by the planet Uranus. The encounter provided space scientists with diverse data on Uranus and its nearby environment [*Stone and Miner*, 1986]. Part of that data provided a glimpse of the rich variety of radio phenomena generated by the interaction between the solar wind and Uranus' magnetospheric plasma and, more directly related to this paper, possibly between the magnetospheric plasma and one of Uranus' moons.

This paper is particularly concerned with a periodic radio emission detected by Voyager at about 700 kilohertz shortly after closest approach. The Planetary Radio Astronomy (PRA) experiment package on Voyager collected these data at about noon (universal time) on 25 January 1986. Figure 1 is a frequency-time spectrogram of the PRA data showing the radio bursts, termed "vertex-early arcs" because they are roughly arc-shaped, with the vertex of each arc occurring first in time, followed by the remainder of the arc. The strongest arcs occur at about 1230 UT, although the arcs begin at a little before 1130 UT and continue to approximately 1300 UT. It is difficult to be certain when the arcs end because of interference from the "smooth high-frequency" emission (SHF [*Leblanc et al.*, 1987]) which begins at about 1300 UT. The periodicity of the arcs varies between about 570 to 600 seconds.

Since the shape of the arcs is discussed elsewhere [*Gurnett and Goertz*, 1981], we will only examine the proposition that the periodic nature of the arcs is caused by Alfvén waves, generated by one of the Uranian moons, propagating along magnetic field lines and reflecting at the ionosphere back again into the magnetosphere. The ionosphere reflects the Alfvén waves many times to produce a multiplicity of arcs. This model, the Alfvén wave multiple-reflection model, has been proposed previously [*Gurnett and Goertz*, 1981] to explain similar radio events at Jupiter, the Jovian decametric radio arcs.

To investigate the plausibility of the multiple-reflection model at Uranus, one needs to explain two things: why Voyager detected the arcs when it did and why their periodicity is (approximately) 600 seconds. Therefore this investigation splits naturally into two parts. The first part of this paper examines the moon-planet-spacecraft geometry. This analysis alone indicates quite specifically what can and what cannot be happening, which moons can and which cannot be responsible for Alfvén wave generation, and where (in which magnetic hemisphere) the radio sources must be located. Geometric considerations also affect the observed period of the arcs, since Voyager, the observer of the arcs, is moving quite rapidly. However, a major requirement for modelling the arc periodicity is an estimate of the propogation times of Alfvén waves in the Uranian magnetosphere. So the second part of this paper develops a crude, but workable, model of the Uranian magnetospheric plasma density and combines the density model with the offset, tilted dipole (OTD) model [*Ness et al.*, 1986] for Uranus' magnetic field. This combination produces the estimate of the Alfvén velocity which, together with the fact that the path of an Alfvén wave is along a magnetic field line, provides sufficient

information to test the plausibility of the Alfvén wave multiple-reflection model with regard to the hectometric arcs.

CHAPTER II

REVIEW OF PREVIOUS WORK

Excitation of Alfvén waves by Unipolar Induction

The generation of Alfvén waves by a conductor moving through a magnetized plasma was first applied to the calculation of ionospheric drag on the Echo 1 satellite [*Drell et al.*, 1965]. It also applies to the moons in the magnetospheres of the outer planets. The motion of the satellite induces a charge separation which the surrounding plasma conducts away along magnetic field lines. Figure 2 illustrates the situation schematically. The charge separation and current in the satellite drive the generation of Alfvén waves described by

$$\left(\mu_0\epsilon_\perp\omega^2 - \frac{\epsilon_\perp}{\epsilon_\parallel}k_\perp^2 - k_z^2\right)E_\perp^\ell = ik_\perp\frac{\rho}{\epsilon_\parallel} - i\omega\mu_0 J_\perp^\ell \qquad (1a)$$

and

$$\left(\mu_0\epsilon_\perp\omega^2 - \frac{\epsilon_\perp}{\epsilon_\parallel}k_\perp^2 - k_z^2\right)E_z = ik_z\frac{\rho}{\epsilon_\parallel} \qquad (1b)$$

in Fourier transform space with the basis

$$\vec{e}_z = \vec{e}_z \qquad \text{(field-aligned)}$$

$$\vec{e}_\perp^{\,\ell} = \frac{1}{k_\perp}\vec{k}_\perp \qquad \text{(longitudinal)}$$

$$\vec{e}_\perp^{\,tr} = \vec{e}_z \times \vec{e}_\perp^{\,\ell}. \qquad \text{(transverse)}$$

These are driven wave equations with evanescent solutions for $k_\perp \neq 0$ since $\frac{\epsilon_\perp}{\epsilon_\parallel} < 0$. The Alfvén waves then carry the charge away in two current "wings." The plasma itself has an effective "Alfvén conductivity" [*Neubauer*, 1980],

$$\Sigma_A^{\pm} = \frac{1}{\mu_0 v_A \sqrt{1 + M_A^2 \pm 2M_A \sin\theta}} , \tag{2}$$

where

$$M_A = \frac{v_0}{v_A}$$

is the Alfvén Mach number, and the definition of the geometry is shown in figure 3. The impedance match between the unipolar inductor (the satellite or moon) and the surrounding plasma determines the efficiency of the Alfvén wave generation.

Multiple-Reflection Model

In the Alfvén wave multiple-reflection model [*Gurnett and Goertz*, 1981], the moon continuously generates waves as it moves through the magnetospheric plasma. The waves propagate along the magnetic field lines until they reach the ionosphere. The ionosphere reflects the waves, which then travel back along the field lines to the opposite hemisphere. This reflection-propagation process continues, possibly many times, until all of the energy in the wave dissipates. Note that, for small inclinations of the moon's orbit and for small tilts, with respect to the planetary rotation axis, of the magnetic dipole, the Alfvén wave pattern is approximately stationary in the reference frame of the moon, like the bow waves of a boat moving in otherwise calm water.

Somewhere near the ionosphere the maser instability [*Wu and Lee*, 1979] converts part of the Alfvén wave energy into coherent cyclotron radiation. It is

a multi-step process in which the Alfvén waves drive field-aligned currents which produce particle beams which cause the radio emission. Each reflection of an Alfvén wave is then associated, more or less, with a cyclotron radiation source. A large pattern of waves with a multiplicity of reflections provides a multiplicity of radio sources. Figure 4 shows, in a single L shell and in a three-dimensional representation, how the multiple reflections produce a pattern of Alfvén waves and multiple radio sources at Jupiter. However, at Jupiter the Io plasma torus complicates the wave geometry in a way that should have no analog at Uranus. Although it is not shown in the diagrams, there could be reflections within the torus itself. Uranus has no torus, so this complication does not arise.

Each of the radio sources produces not an isotropic distribution of radiation, but a conical, hollow shell of radiation nearly perpendicular to the magnetic field. The condition of perpendicularity is consistent with the theory of the maser instability [*Wu and Lee*, 1979] and the observations of both the Jovian decametric arcs [*Gurnett and Goertz*, 1981] and the broadband bursty (b-bursty) events at Uranus [*Farrell and Calvert*, 1988]. Since the geometry is time dependent and may involve observer motion as well as source motion, a sequence of these conical shells may include the observer position. Voyager 2, a mechanical observer in this case, receives radio energy when it is on a shell and receives nothing when it is not on a shell. The thinness of the radiation cone and the motion of the Alfvén pattern with the moon then explain the discreteness of the arcs. The multiplicity of reflections, and therefore radio sources, explains the multiplicity of the arcs.

CHAPTER III

GEOMETRY

Horizon and Radiation Cone Angles

If we are to test the plausibility of the multiple-reflection model, we should first see whether or not Voyager could have seen any radio emissions if they did happen to be present. Assuming that the radio energy is beamed in a cone from the moon's magnetic flux tube at a point where the local electron cyclotron frequency equals the emission frequency, we need to check two things: did Uranus (or actually a shell of constant cyclotron frequency) physically obstruct the line-of-sight from Voyager to the emission point, and what was the opening angle of the radiation cone? We do this by calculating the angle between the line-of-sight and the local vertical, the horizon angle, and the angle between the line-of-sight and the local magnetic field vector, the radiation cone angle. Figure 5 illustrates these definitions. By the definition of the horizon angle, there is a clear line-of-sight for horizon angles less than 90 degrees. Recall the cyclotron resonance of the maser instability causes the radiation cone angle to be approximately 90 degrees, perpendicular to the magnetic field.

We consider only the the three innermost moons, Miranda, Ariel, and Umbriel, as possible Alfvén wave unipolar generators. The positions of the moons during the time at which Voyager detected the arcs are known. Since Alfvén waves travel only along magnetic field lines, the magnetic longitude of the emission point must

be either the magnetic longitude of the moon or at least a magnetic longitude in the moon's recent past, since that is where the Alfvén waves are. Matching the observed radio frequency with the electron cyclotron frequency fixes the magnetic latitudes (north and south) of the possible emission points. Figure 6 illustrates the magnetometer (MAG) latitude convention [*Ness et al.*, 1986] and the magnetic longitude convention this paper adopts. Tables 1–3 then show the positions of Voyager and the three innermost moons during the period of time coincident with the arcs.

One might argue that, for the simplest consideration, we could take the possible emission point longitudes as simply equal to those of the flux tubes of the various moons. We then calculate the horizon angles and required radiation cone angles for these points. The horizon angles are plotted as a function of time in figure 7 for the upper and lower frequencies to which the arcs extend. Figure 8 shows the radiation cone angles as a function of time. However, because of the unreasonable assumption that the emission point coincides in longitude with the moon, the only information obtained from these plots is that the emission point is in the southern magnetic hemisphere. The necessary radiation cone angle for a northern emission point is much too small by our previous, reasonable assumption that the radiation cone angle should be near 90 degrees. If the Alfvén waves propagate back and forth along their respective magnetic field lines (due to multiple reflections), then the emission point can be anywhere the moon has just been.

What we must really do is consider each pair of spacecraft/moon coordinates, whether they are temporally coincident or not. Such a consideration is a little bit more complicated. In figures 9 – 12 time is no longer explicit. The magnetic

longitudes are alone sufficient to represent the coordinates of the moon and spacecraft. For each pair of coordinates, the horizon angles and radiation cone angles are calculated. The diagrams are then contours of constant horizon angle and constant radiation cone angle in degrees. The dashed lines are spacecraft longitude plotted against moon longitude. Since both Voyager and any of the moons in question are increasing in longitude with time, the area to right of the dashed line represents the future. We are not interested in that region, since no valid solution exists there. The area to the left of the dashed line represents the recent past, where valid solutions exist.

Notice that in every diagram, the horizon angle contours to the left of the dashed line have values less than 90 degrees. As in the simplistic examination with the emission point longitudes equal to those of the flux tubes, all of the possible emission points are visible. It is the constraint on the radiation cone which limits the possibilities most tightly. The strongest arcs occurred between 1200 and 1250 universal time, when Voyager was between 207 and 212 degrees east magnetic longitude. For the cone angle contour diagrams the requirement that the cone angle be approximately 90 degrees translates to one in which horizontal lines corresponding to 207 and 212 degrees spacecraft longitude must intersect common contours in the neighborhood of 90 degrees, which they must do to the left of the dashed line. These intersections occur in only two of the six cases.

For Alfvén wave generation by either Miranda or Ariel, points near flux tube feet in the southern magnetic hemisphere of Uranus are geometric possibilities for the location of the radio sources of the arcs. Of course in both cases it is not the moons' current flux tubes which may be associated with the radio emissions, but

flux tubes through which they have recently passed. In either case one conclusion is very definite: if the Alfvén wave multiple-reflection mechanism is responsible for the observed arcs, the radiation must come from Uranus' southern magnetic hemisphere. The height of the 700 kHz emission point is about 1.2 R_U from the dipole center, or about 1.1 R_U from the planet center. If Miranda is the generator, these geometric considerations limit the radiation cone very tightly to about 82 degrees. If Ariel is the generator, the radiation cone is about 87 to 90 degrees. To determine more clearly which of these two cases is responsible for the arcs, we need to compare a calculated periodicity, given the geometry, with the observed periodicity. This comparison is done in a later section of this paper.

Polarization

The origin of the electron cyclotron radiation in the southern magnetic hemisphere would cause the arcs to have a definite polarization, uniform from arc to arc. The PRA instrument itself detects the separate circular polarizations, using the radio science convention to describe the sense of the polarization. The radio science convention is different from the one normally used by plasma physicists.

The plasma physics convention describes the rotation of the wave electric field with respect to the static magnetic field. If one points his thumb in the direction of the magnetic field, the electric field of a circularly polarized wave rotates in the direction which the fingers of that hand point. In this convention electron cyclotron radiation is always right-hand polarized at the source.

The radio science convention describes the rotation of the electric field with respect to the wavevector. If one points his thumb in the direction of propagation,

the electric field of a circularly polarized wave rotates in the direction which the fingers of that hand point. The optical convention also describes the rotation of the electric field with respect to the wavevector, but it is exactly the opposite of the radio science convention. In the radio science convention, electron cyclotron radiation from the southern magnetic hemisphere of Uranus should be right-hand circularly polarized.

Figure 13 shows the two components in decibels, averaged over frequency, for the arcs using the radio science convention. The barely predominant polarization of the spikes, which are the arcs, is right-hand. The lack of clear dominance occurs because the direction to Uranus from Voyager is very nearly in the electrical plane of the PRA antennae [*Leblanc et al.*, 1987]. The arcs do appear to have a slight, uniform polarization, however: corroborating evidence, albeit a little uncertain, that the emissions originate consistently from the southern magnetic hemisphere of Uranus.

Spacecraft Motion

As the pattern of Alfvén waves follows the moon around the planet, points approximately equally spaced along the track of the foot of the flux tube would illuminate a stationary observer at intervals equal to the time required for one north-south propagation of an Alfvén wave. However, Voyager is not stationary. We therefore need to see how this fact alters the simple north-south propagation periodicity which a stationary observer expects. Consider two adjacent actual emission points and a geometrically favorable point in their vicinity, shown schematically in figure 14.

The actual emission points are moving along the track of the moon's flux tube at approximately the same velocity which the moon's flux tube had when it was there. The geometrically favored point has some other velocity. When an emission point coincides with the geometrically favored point, Voyager receives a radio arc. Assume the velocities of the adjacent emission points are equal. This condition is only approximately true because the velocity of the moon's ground trace will vary as the moon varies in latitude. It is still a fair assumption because the moon will not vary much in latitude in the time it takes for a single Alfvén wave reflection cycle. Further assume that the velocity of the geometrically favored point is a constant between the two emission points. This condition is also only approximate, but it is still another fair assumption. We would expect that the emission points are spaced closely enough that the moon-planet-spacecraft geometry would not change radically in the time it takes for the favored point to move from one radiation source to the next. If v and v' are the velocities of the geometrically favored point and the emission points respectively, and if τ is the Alfvén period for one north-south propagation cycle, then the observed periodicity is

$$T = \frac{\tau v'}{v - v'} = \left[\frac{1}{\left(\frac{v}{v'}\right) - 1} \right] \tau \ . \tag{3}$$

The quantity in square brackets is a purely geometric effect. A negative value of T just means that the observer sees images generated at earlier and earlier times. Tables 4–5 shows the results of calculations of this geometrical factor assuming Miranda and Ariel generate the waves, with the emission point located in the southern magnetic hemisphere.

Minimum Required Alfvén Delay

As the initial Alfvén disturbance propagates away from the moon and, after reflection, back towards the moon, the moon continues to revolve about the planet. The moon must not intercept the reflected Alfvén wave if the wave is to continue propagating to the opposite hemisphere, thus beginning the multiple-reflection process. In other words, the moon must get out of the way of the reflected wave for the multiple-reflection model to be valid. Whether this last geometrical requirement is satisfied may be time dependent because of the large inclination between Uranus' magnetic equatorial plane and the moons' orbital planes. The orbits of the moons are inclined 60.1 degrees with respect to the magnetic axis of Uranus. Ignoring the offset of the dipole, both Miranda and Ariel will vary in magnetic latitude between 60 degrees north and 60 degrees south.

Consider a coordinate system where the dipole (ignoring the small offset) is in the xz-plane, where the z-axis is the rotation axis. If the dipole tilt is an angle α, then to transform from the rotational frame to the magnetic frame we use a simple vector rotation.

$$R = \begin{bmatrix} \cos\alpha & 0 & -\sin\alpha \\ 0 & 1 & 0 \\ \sin\alpha & 0 & \cos\alpha \end{bmatrix} \tag{4}$$

Assume a circular orbit for the moon to simplify the mathematics. Define $t = 0$ when the moon is along the positive x-axis. Then the position of the moon is

$$\vec{r} = r \begin{bmatrix} \cos\omega t \\ \sin\omega t \\ 0 \end{bmatrix}, \tag{5}$$

where r is the orbital radius of the moon and

$$\omega = \omega_{moon\ orbit} - \omega_{planet\ rotation}$$

is the effective angular velocity of the moon. Rotate the position vector into the magnetic frame.

$$\vec{r}\,' = \begin{bmatrix} \cos\alpha\cos\omega t \\ \sin\omega t \\ \sin\alpha\cos\omega t \end{bmatrix} \tag{6}$$

$$\cos\theta = \sin\alpha\cos\omega t$$

$$\tan\phi = \sec\alpha\tan\omega t$$

where θ = magnetic polar latitude and ϕ = magnetic east longitude. With a little bit of algebra, we can get

$$\frac{d\phi}{dt} = \omega\frac{\cos\alpha}{\sin^2\theta}\ . \tag{7}$$

If D is the diameter of the moon, then its angular width (in longitude) from the center of the planet is

$$\delta = \frac{D}{r\sin\theta}\ . \tag{8}$$

This is exactly the angular distance the moon must move in order that it does not intercept the first reflected Alfvén wave. To allow this, the minimum required delay is

$$t_{req} = \frac{\delta}{\frac{d\phi}{dt}} = \left(\frac{D}{r\omega\sin\alpha}\right)\sin\theta$$

$$= t_{req}^{max}\sin\theta\ . \tag{9}$$

Using typical values [*Stone and Miner*, 1986] for the parameters D, r, and ω, we get

$$Miranda\ :\ t_{req}^{max} = 152.0\ sec$$

$$Ariel\ :\ t_{req}^{max} = 169.6\ sec\ .$$

After we calculate a predicted propagation delay for waves generated by either moon, we can compare that delay to the minimum required delay. We expect this result to be significant because the arcs are evenly spaced in time (fig. 1). If both the Alfvén wings produced multiple reflections, the radio arcs would occur in evenly spaced pairs. Since the arcs do not occur in pairs, we can expect to find that the moon, whichever one is the generator, intercepts the reflection from the nearest reflection point. This observation must be consistent with the total periodicity. So we therefore turn our attention to the calculation of Alfvén propagation times in the Uranian magnetosphere.

CHAPTER IV

ALFVÉN BOUNCE PERIOD

Density Dependence

Simply stated, the Alfvén waves travel along magnetic field lines, which are not straight, at velocities which are not constant. This presents no great impediment by itself, however. Just note that

$$dt = \frac{ds}{v_A} \tag{10}$$

and

$$v_A = \frac{B}{\sqrt{\mu_\circ \rho}} ,$$

where ds is a differential of path length and ρ is the mass density. For a path along a dipolar field line

$$\begin{aligned} ds &= \sqrt{dr^2 + r^2 d\theta^2} \\ &= \ell \sin\theta \sqrt{1 + 3\cos^2\theta}\; d\theta , \end{aligned} \tag{11}$$

where, for convenience, $\ell = LR_U$ if L is the conventional L-shell parameter. Combine this with

$$\begin{aligned} B &= \sqrt{B_r^2 + B_\theta^2} \\ &= \frac{\mu}{r^3} \sqrt{1 + 3\cos^2\theta} , \end{aligned} \tag{12}$$

where μ is the magnetic dipole moment, to get

$$t = \ell^4 \frac{\sqrt{\mu_o}}{\mu} \int_{\theta_i}^{\theta_f} \sqrt{\rho} \sin^7 \theta \, d\theta \,, \tag{13}$$

expressing $\rho = \rho(\ell, \theta)$ to integrate along a field line. Equation 13 expresses the propagation time between any two points on a field line in general. The total Alfvén bounce period is

$$\tau = 4\ell^4 \frac{\sqrt{\mu_o}}{\mu} \int_{\theta_{ion}}^{\frac{\pi}{2}} \sqrt{\rho} \sin^7 \theta \, d\theta \,, \tag{14}$$

where θ_{ion} is the colatitude where the magnetic field line intersects the base of the ionosphere.

Since the magnetic moment is known [*Ness et al.*, 1986], and since the positions and the path are specified, any propagation times only depend upon how we model the plasma density in the Uranian magnetosphere. Unfortunately there is very little plasma density data. At this point it is worthwhile to remember that the objective is only to test the plausibility of the Alfvén wave multiple-reflection model at Uranus. We do not want an elaborate plasma density model which takes a large variety of magnetospheric processes into account. We aim at a minimal model with at least some physical justification, realizing that any extra complexity would not yield any significantly better results, especially given the uncertainty in extrapolation of the density data to the entire magnetosphere.

Back of the Envelope Estimate

The simplest thing to do is just to assume a constant density everywhere. The next simplest is to assume a constant magnetospheric density and introduce a simple ionospheric density model. Making the total Alfvén period (τ in equation 14) for

the Alfvén waves be near the observed period of the arcs (about 600 seconds), we can work backwards to determine the required plasma density. For the moment we can neglect the geometric effect on the observed period (equation 3), because the correction factors are on the order of unity (tables 4–5). If the plasma consists only of a single species, then the mass density ρ depends only upon the number density n.

Under the assumption that the plasma is entirely atomic hydrogen [*Bridge et al.*, 1986], the simplest calculation mentioned above yields, for three different L values, densities, shown in table 6, on the order of 1 to 10 cm^{-3}, which are comparable to those inferred from plasma (PLS) observations [*Bridge and Belcher*, 1986] during the Uranus encounter. Over a four hour interval near closest approach, the density varied between about 0.3 cm^{-3} and about 2.4 cm^{-3}. The approximate correspondence between observation and simple calculation means that the Alfvén wave multiple-reflection mechanism could be plausible. We are encouraged to try the second simple calculation mentioned above, separating the ionosphere from the magnetosphere.

The data from the encounter indicate a magnetospheric number density of about 1 cm^{-3}, so assume a magnetospheric density of 1 cm^{-3}. For the ionosphere we assume a "slab" model with a thickness given by the scale height

$$H = \frac{2kT_o R_U^2}{GMm} = 0.0584\ R_U, \tag{15}$$

where $T_o = 800\ K$, derived from the ultraviolet spectroscopy (UVS) experiment as the temperature of the neutral ionosphere [*Herbert et al.*, 1987]. There is an extra factor of 2 in the plasma scale height as compared to the neutral scale height because

of the ambipolar electric field resulting from minute charge separations. The results of calculating the required ionospheric density for a 600 second period, also shown in table 6, are either high, if comparison of Uranian densities to Saturnian ones of about $10^5\ cm^{-3}$ [*Kaiser et al.*, 1984] is valid, or just simply ridiculous. This result shows that one should concentrate on the magnetospheric density. The time delay introduced by the ionospheric density is negligible. It is important to note that the ionospheric density may still remain significant as a boundary condition on the magnetospheric density.

Non-Rotational Model

A simple model for the plasma density is a scale height model of the form

$$n = n_\infty e^{\frac{H}{r}}, \tag{16}$$

where $H = \frac{1}{2}GMm\beta_\circ$ and $\beta_\circ = \frac{1}{kT_\circ}$. Equation 16 is a solution to the barometric equation

$$kT\nabla n = -\rho\nabla\phi\ , \tag{17}$$

where

$$\phi = -\frac{GM}{2r}$$

is the gravitational potential, with an extra factor of 2 for the ambipolar electric field. The implicit assumptions in this model are that the plasma is in collisional equilibrium with the ionosphere and that the centrifugal force is negligible. We can re-express the density as

$$n = n_o e^{H\left(\frac{1}{r}-\frac{1}{r_o}\right)}, \tag{18}$$

where $n_o = n\Big|_{r=r_o}$. We may let r_o be anything, but it is most meaningful to let $r_o = 1\ R_U$. This leaves n_o, the ionospheric density, and β_o (and thus H) as the free parameters. Rather than allowing β_o to vary freely, we can specify a series of values and find the corresponding series of n_o values which fits the data best for least square error. Convenient units of β are $1 \times 10^{34}\ sec^2 - kg^{-1} - R_U^{-2}$. For $T_o = 800\ K$, $\beta_o = 5.94 \times 10^{34}\ sec^2 - kg^{-1} - R_U^{-2}$. Table 7 shows the values of n_o that best fit the data, given the values of β_o. Figure 15 shows a typical fit to data as a function of L shell.

Note that in the data, for a given L value, the measured density values are higher as Voyager is outbound from Uranus than when it is inbound. Since Voyager is closer to the magnetic equator on the outbound passage, the increase in density is most likely indicative of centrifugally trapped particles. We take up this point in the next model for consideration. Now it is sufficient to note that the fits are not very good and that, even qualitatively, the shape of the curve confuses on which pass, inbound or outbound, the density should be higher. We may nevertheless calculate the total Alfvén propagation period as a function of generator latitude. Figure 16 shows a typical case of the Alfvén period variation with latitude. Figure 17 summarizes these calculations in a plot of the period for a generator in the magnetic equatorial plane as a function of modelled ionospheric density.

There is a clear trade-off between a cold, dense ionosphere and a hotter, less dense ionosphere as a boundary condition. Although the predicted Alfvén period is within an order of magnitude of the observed period of the radio arcs and the required ionospheric densities are slightly high, the major inadequacy of this model

is its failure to fit the data qualitatively (fig. 15). However, the results are still encouraging enough to try one final model.

Spin-Aligned Model

For this model we will begin with the assumptions that: (1) the plasma is entirely hydrogen [*Bridge et al.*, 1986]; (2) the plasma particles are constrained to move only along magnetic field lines; (3) in the magnetosphere the plasma is collisionless; and (4) the only forces acting on the particles are gravitational and centrifugal. In a collisionless plasma, we may not assume a uniform temperature or even a Maxwellian velocity distribution. This means we cannot use the barometric equation (equation 17), where ϕ is the conservative potential including both gravitational and centrifugal parts, as has been done for the Jovian magnetosphere [*Gledhill*, 1967].

Instead, we will divide the space around Uranus into three parts: a spherically symmetric extended ionosphere, a gravitationally dominated inner magnetosphere, and a centrifugally dominated outer magnetosphere, all shown schematically in figure 18. The ionosphere is collisional and isothermal. Therefore, it is described by equation 18. Its temperature and height (r_o) are free parameters, as is the number density (n_o) at the "top" of the ionosphere. Particles travelling collisionlessly along the magnetic field lines populate the inner magnetosphere. Those particles with the highest energies populate the outer magnetosphere along with lower energy particles trapped in the centrifugal well. Figure 19 illustrates the centrifugal well in the potential as it varies along a magnetic field line. The particles trapped in the outer magnetosphere are also collisionless.

The model uses magnetic longitude and magnetic colatitude throughout, so the implicit mathematical simplification is that the rotation axis is dipole-aligned. Viewed another way, one could say that the dipole is spin-aligned in this simple model. This may already seem to invalidate the model, but the vast simplification it allows justifies the attempt to model the plasma this way. Note that this model is an especially reasonable approximation near the intersection of the magnetic equatorial plane and the rotational equatorial plane (90 degrees and 270 degrees magnetic longitude). Both Miranda and Ariel are near 270 degrees magnetic longitude. One might also choose to work in centrifugal coordinates, where the symmetry surface is the plane of the centrifugal equator [*Hill et al.*, 1974] rather than the plane of the rotational equator or the magnetic equator. However, we will use magnetic coordinates exclusively.

Let V be the potential energy of a proton in the magnetosphere, including both the gravitational and centrifugal parts. Define $V = 0$ at the top of the ionosphere for any particular magnetic field line. Then for any particle with mass m

$$v_{\parallel}^2 = v_{\parallel\circ}^2 - \frac{4}{m}V \tag{19}$$

is just conservation of energy, ignoring the effect of the magnetic field through adiabatic invariants, but including the effect of the ambipolar electric field, which can be interpreted as altering the effective mass of the ions. The ionosphere is collisional, so the particles there are Maxwellianly distributed.

$$f(v_{\parallel\circ}) = \sqrt{\frac{m\beta_\circ}{4\pi}} e^{-\frac{1}{4}m\beta_\circ v_{\parallel\circ}^2} \tag{20}$$

$$\beta_\circ = \frac{1}{kT_\circ}$$

According to Liouville's Theorem, the phase space density remains constant with evolution. Therefore we may just use the conservation of energy to transform the velocity coordinate correctly from one region of configuration space to another. Integrating the distribution function over all velocities at any point in space yields the number density there.

$$n_{inner} = 2n_\circ \sqrt{\frac{m\beta_\circ}{4\pi}} \int_{\sqrt{\frac{1}{m}V}}^{\infty} e^{-\frac{1}{4}m\beta_\circ v_{\|\circ}^2}\, dv_{\|\circ} \ , \tag{21}$$

where $n_\circ$ is the number density at the top of the ionosphere.

$$n_{inner} = n_\circ \operatorname{erfc}\left(\sqrt{\beta_\circ V}\right) \tag{22a}$$

$$n_{outer} = n_\circ \operatorname{erfc}\left(\sqrt{\beta_\circ V_{max}}\right) \tag{22b}$$

To get n_{outer} we simply realize that all particles with an energy above the maximum value of the potential, denoted V_{max}, are the only particles energetic enough to make it across the potential barrier into the outer magnetosphere. Note that V_{max} is a constant for any given magnetic field line, therefore n_{outer} is a constant for any given magnetic field line. If $r_\circ$ is the height of the ionosphere from the center of the planet, then the potential is

$$V = \frac{1}{2}\left[GMm\left(\frac{1}{r_\circ} - \frac{1}{r}\right) + \frac{1}{2}m\omega^2\frac{1}{\ell}\left(r_\circ^2 - r^3\right)\right] \ , \tag{23}$$

where here $\omega = \omega_{planet}$. Maximizing this potential, we find that the colatitudes which divide the inner from the outer magnetosphere are described by

$$\sin^2\theta_B = \left[\frac{2GM}{3\omega^2\ell^3}\right]^{\frac{1}{4}} . \tag{24}$$

$$V_{max}(\ell) = \frac{1}{2}\left\{\frac{GMm}{r_\circ} + \frac{1}{2}m\omega^2\frac{r_\circ}{\ell} - m\left[\frac{128(GM)^3\omega^2}{27\ell}\right]^{\frac{1}{4}}\right\} \tag{25}$$

Recall that n_o , β_o , and r_o are the free parameters in this model.

Equations 22–25 describe the particles with an ionospheric origin. There is also a trapped distribution in the centrifugal well. We would like to maintain mathematical simplicity, but the distribution function should be continuous between the trapped and untrapped particles. An easy way to satisfy both requirements is to simply say that the trapped distribution is a constant at the magnetic equator, where V has a local minimum, V_{min} .

$$V_{min} = \frac{1}{2}\left[GMm\left(\frac{1}{r_o} - \frac{1}{\ell}\right) + \frac{1}{2}m\omega^2\frac{1}{\ell}\left(r_o^2 - \ell^3\right)\right] \tag{26}$$

The equatorial trapped distribution is

$$f_e(v_\parallel)\Big|_{v_{\parallel o}^2 = \frac{4}{m}V_{max}} = \sqrt{\frac{m\beta_o}{4\pi}}\; e^{-\beta_o V_{max}}. \tag{27}$$

Once again integrate this distribution function over all sensible velocities to obtain the number density.

$$n_{trapped} = 2n_o \int_{\sqrt{\frac{4}{m}(V - V_{min})}}^{\sqrt{\frac{4}{m}(V_{max} - V_{min})}} \sqrt{\frac{m\beta_o}{4\pi}}\; e^{-\beta_o V_{max}}\; dv_{\parallel e} \tag{28}$$

The integration is over the equatorial velocities of the trapped particles.

$$n_{trapped} = n_o\sqrt{\frac{4\beta_o}{\pi}}\left(\sqrt{V_{max} - V_{min}} - \sqrt{V - V_{min}}\right) \tag{29}$$

As with the non-rotational model we specify a series of values to β_o and find the corresponding values of r_o and n_o which minimize the mean square error to the PLS data. Table 8 shows these values. Figure 20 shows a typical fit to the data as a function of L shell. Qualitatively and quantitatively the shape of the curves is

quite good. A more involved model of the trapped distribution might improve the fit, but recall that we want to retain a simple model.

We may again calculate the total Alfvén propagation period as a function of generator latitude, shown for a typical case in figure 21, and summarize the results by plotting the period for a generator in the magnetic equatorial plane as a function of modelled ionospheric density, which is what figure 22 does. The predicted period, if Miranda is the Alfvén generator, falls short of the desired 600 second period by a factor of over six, but within an order of magnitude. However if Ariel is the generator, the predicted period falls short by a factor of about two. The case for Ariel seems quite reasonable given all the simplifications employed.

Final Checks

We still need to justify why the observed periodicity of the radio arcs should correspond to the Alfvén periodicity and not half of the Alfvén periodicity, since a moon would generate two Alfvén wings. We should also combine the geometric factors which would affect the observed periodicity with the periods calculated from the density model.

Recall that in the discussion of a required propagation delay (t_{req} in equation 9), the condition arises that the moon must move quickly enough to get out of the path of its own reflected Alfvén wave. It so happens that Ariel is in the northern magnetic hemisphere as Voyager receives the radio arcs. The Alfvén wave which propagates northward has a small enough transit time that Ariel intercepts the reflected wave. No multiple reflections can occur from this particular wave. Ariel does not intercept the reflection of the southward generated wave, however, so the southward wave can

indeed set up multiple reflections. Ariel effectively generates only one Alfvén wing. The same thing could occur if Ariel were in the southern magnetic hemisphere. In that case only the northward generated Alfvén wave could reflect multiple times between the northern and southern hemispheres. The reflection time to the near hemisphere is less than the minimum required propagation delay, as figure 23 shows.

Finally, Ariel does not remain at a constant magnetic latitude during the generation of the radio arcs. As it increases in latitude (because its longitude diverges from 270 degrees in table 5), the total Alfvén period increases. But the geometric correction to the period (table 5) is a factor which decreases. Multiplying the Alfvén period which corresponds to Ariel's latitude by the applicable geometric factor for the appropriate time (equation 3) yields the final prediction of the observed period of the radio arcs. Figure 24 is the result of such a calculation using the set of parameters with $\beta_o = 6.0 \times 10^{34}\ sec^2 - kg^{-1} - R_U^{-2}$, or $T_o = 790\ K$ as the ionospheric ion temperature. The actual observed period is reasonably constant at about 600 seconds. The "spin-aligned" model predicts periods of about 300 seconds: nearly constant and a factor of about two from the observed period.

CHAPTER V
CONCLUSION

The Alfvén wave multiple-reflection model proves to explain adequately the vertex-early radio arcs detected at Uranus by Voyager 2. Consideration of the three innermost large moons, Miranda, Ariel, and Umbriel, shows that Umbriel is not the Alfvén wave generator for purely geometric reasons. Increasingly complex models of the plasma density in the Uranian magnetosphere rule out Miranda as the generator. It appears that the best possibility is that Ariel is the Alfvén wave generator, if the multiple-reflection model is correct, and that the cone half-opening angle for the arc radiation is about 87 degrees to 90 degrees. Using a nominal value of 88 degrees and the reasonable, although quite simplified, "spin-aligned" model of the Uranian magnetospheric plasma density, we would predict the observed period of the radio arcs should be about 300 seconds. This is a factor of about two from the actually observed period of about 600 seconds.

The discrepancy between the observed and predicted periodicity might possibly be resolved with a more complex model of the plasma density, but this is not certain. Such a model would include, at least, the effects of the 60 degree tilt between the magnetic axis and the rotation axis. It would also include the effect of the magnetic field altering the pitch angles of the plasma particles as they travel along the magnetic field lines. There is also certainly a great deal of room for improvement in the modelling of the centrifugally trapped distribution. However, the additional

work would require additional effort an order of magnitude beyond the scope of this thesis. It is not clear that such an increase in the level of effort would result in an increase in the precision and certainty of the calculations, especially considering the paucity of available data.

However, we might guess that the predicted period could be increased if we were to include the possibility of multiple species of plasma, particularly in the inner magnetosphere. Since anything is more massive than atomic hydrogen, this would slow the Alfvén wave propagation. The other factors included in the considerations, the dipolar magnetic field, the geometric analysis, and the reliability of the instruments involved, are too certain for any gross inaccuracies to exist there. This paper originally began as an investigation of the plausibility of the Alfvén wave multiple-reflection model at Uranus. It is indeed plausible.

Table 1: Uranus Encounter Ephemeris for Voyager and Miranda

Time (UT)	R_{sc} (R_U)	S/C Mag Lat (deg)	S/C Mag Long (deg)	R_{moon} (R_U)	Miranda Mag Lat (deg)	Miranda Mag Long (deg)
25 1115	37.64	7.60	201.68	5.11	-41.09	246.36
25 1120	37.82	8.16	202.39	5.11	-40.37	246.98
25 1125	37.99	8.73	203.09	5.11	-39.64	247.58
25 1130	38.17	9.31	203.77	5.11	-38.92	248.17
25 1135	38.34	9.92	204.43	5.11	-38.19	248.74
25 1140	38.52	10.54	205.09	5.10	-37.46	249.31
25 1145	38.69	11.17	205.73	5.10	-36.72	249.87
25 1150	38.87	11.83	206.35	5.10	-35.98	250.42
25 1155	39.04	12.49	206.96	5.10	-35.25	250.95
25 1200	39.22	13.18	207.56	5.10	-34.51	251.48
25 1205	39.39	13.88	208.14	5.10	-33.76	252.00
25 1210	39.57	14.59	208.71	5.10	-33.02	252.52
25 1215	39.75	15.31	209.25	5.10	-32.27	253.02
25 1220	39.92	16.05	209.79	5.10	-31.53	253.52
25 1225	40.10	16.80	210.30	5.10	-30.78	254.01
25 1230	40.27	17.57	210.80	5.10	-30.03	254.49
25 1235	40.45	18.34	211.28	5.10	-29.27	254.97
25 1240	40.62	19.13	211.75	5.09	-28.52	255.44
25 1245	40.80	19.93	212.20	5.09	-27.77	255.91
25 1250	40.97	20.73	212.62	5.09	-27.01	256.36
25 1255	41.15	21.55	213.04	5.09	-26.25	256.82
25 1300	41.32	22.38	213.43	5.09	-25.50	257.27
25 1305	41.50	23.22	213.80	5.09	-24.74	257.71
25 1310	41.67	24.06	214.15	5.09	-23.98	258.15
25 1315	41.85	24.92	214.48	5.09	-23.22	258.59
25 1320	42.02	25.78	214.80	5.09	-22.46	259.02
25 1325	42.20	26.65	215.09	5.09	-21.69	259.44
25 1330	42.37	27.52	215.36	5.09	-20.93	259.87
25 1335	42.55	28.40	215.61	5.09	-20.17	260.29

Table 2: Uranus Encounter Ephemeris for Voyager and Ariel

Time (UT)	R_{sc} (R_U)	S/C Mag Lat (deg)	S/C Mag Long (deg)	R_{moon} (R_U)	Ariel Mag Lat (deg)	Ariel Mag Long (deg)
25 1115	37.64	7.60	201.68	7.47	2.37	274.05
25 1120	37.82	8.16	202.39	7.47	3.44	274.67
25 1125	37.99	8.73	203.09	7.47	4.52	275.31
25 1130	38.17	9.31	203.77	7.47	5.59	275.94
25 1135	38.34	9.92	204.43	7.47	6.66	276.58
25 1140	38.52	10.54	205.09	7.47	7.74	277.22
25 1145	38.69	11.17	205.73	7.47	8.81	277.86
25 1150	38.87	11.83	206.35	7.47	9.87	278.51
25 1155	39.04	12.49	206.96	7.47	10.94	279.16
25 1200	39.22	13.18	207.56	7.47	12.01	279.83
25 1205	39.39	13.88	208.14	7.47	13.07	280.49
25 1210	39.57	14.59	208.71	7.47	14.13	281.17
25 1215	39.75	15.31	209.25	7.47	15.19	281.85
25 1220	39.92	16.05	209.79	7.47	16.24	282.54
25 1225	40.10	16.80	210.30	7.47	17.30	283.23
25 1230	40.27	17.57	210.80	7.46	18.35	283.94
25 1235	40.45	18.34	211.28	7.46	19.39	284.65
25 1240	40.62	19.13	211.75	7.46	20.44	285.38
25 1245	40.80	19.93	212.20	7.46	21.48	286.12
25 1250	40.97	20.73	212.62	7.46	22.51	286.87
25 1255	41.15	21.55	213.04	7.46	23.55	287.63
25 1300	41.32	22.38	213.43	7.46	24.57	288.40
25 1305	41.50	23.22	213.80	7.46	25.60	289.19
25 1310	41.67	24.06	214.15	7.46	26.61	289.99
25 1315	41.85	24.92	214.48	7.46	27.63	290.81
25 1320	42.02	25.78	214.80	7.46	28.64	291.65
25 1325	42.20	26.65	215.09	7.46	29.64	292.50
25 1330	42.37	27.52	215.36	7.46	30.63	293.37
25 1335	42.55	28.40	215.61	7.46	31.62	294.26

Table 3: Uranus Encounter Ephemeris for Voyager and Umbriel

Time (UT)	R_{sc} (R_U)	S/C Mag Lat (deg)	S/C Mag Long (deg)	R_{moon} (R_U)	Umbriel Mag Lat (deg)	Umbriel Mag Long (deg)
25 1115	37.64	7.60	201.68	10.39	-60.25	159.62
25 1120	37.82	8.16	202.39	10.39	-60.66	162.41
25 1125	37.99	8.73	203.09	10.39	-61.00	165.26
25 1130	38.17	9.31	203.77	10.39	-61.29	168.17
25 1135	38.34	9.92	204.43	10.39	-61.51	171.13
25 1140	38.52	10.54	205.09	10.39	-61.67	174.12
25 1145	38.69	11.17	205.73	10.39	-61.77	177.14
25 1150	38.87	11.83	206.35	10.39	-61.80	180.16
25 1155	39.04	12.49	206.96	10.39	-61.76	183.19
25 1200	39.22	13.18	207.56	10.39	-61.66	186.21
25 1205	39.39	13.88	208.14	10.39	-61.50	189.20
25 1210	39.57	14.59	208.71	10.39	-61.27	192.15
25 1215	39.75	15.31	209.25	10.39	-60.98	195.05
25 1220	39.92	16.05	209.79	10.39	-60.62	197.90
25 1225	40.10	16.80	210.30	10.39	-60.21	200.68
25 1230	40.27	17.57	210.80	10.39	-59.75	203.39
25 1235	40.45	18.34	211.28	10.39	-59.23	206.02
25 1240	40.62	19.13	211.75	10.39	-58.66	208.56
25 1245	40.80	19.93	212.20	10.39	-58.05	211.03
25 1250	40.97	20.73	212.62	10.39	-57.39	213.41
25 1255	41.15	21.55	213.04	10.39	-56.68	215.70
25 1300	41.32	22.38	213.43	10.39	-55.94	217.91
25 1305	41.50	23.22	213.80	10.39	-55.16	220.03
25 1310	41.67	24.06	214.15	10.39	-54.34	222.07
25 1315	41.85	24.92	214.48	10.39	-53.50	224.03
25 1320	42.02	25.78	214.80	10.39	-52.62	225.92
25 1325	42.20	26.65	215.09	10.39	-51.72	227.73
25 1330	42.37	27.52	215.36	10.39	-50.78	229.47
25 1335	42.55	28.40	215.61	10.38	-49.83	231.14

Table 4: Geometric Factors for Waves Generated by Miranda

Time (UT)	Source Magnetic Longitude (deg)	Delta Source Longitude (deg)	Delta Miranda Longitude (deg)	Geometric Factor
025 1150	224.846			
		3.212	1.258	0.644
025 1155	228.058			
		3.131	1.276	0.687
025 1200	231.190			
		2.966	1.293	0.772
025 1205	234.156			
		2.829	1.309	0.861
025 1210	236.985			
		2.705	1.324	0.959
025 1215	239.690			
		2.648	1.339	1.023
025 1220	242.338			
		2.743	1.354	0.975
025 1225	245.082			
		2.917	1.370	0.885
025 1230	247.999			
		2.991	1.386	0.864
025 1235	250.990			
		4.396	1.407	0.471
025 1240	255.386			

Table 5: Geometric Factors for Waves Generated by Ariel

Time (UT)	Source Magnetic Longitude (deg)	Delta Source Longitude (deg)	Delta Ariel Longitude (deg)	Geometric Factor
025 1120	274.236			
		-0.140	0.791	-0.850
025 1125	274.096			
		-0.182	0.790	-0.813
025 1130	273.914			
		-0.256	0.790	-0.755
025 1135	273.659			
		-0.279	0.789	-0.738
025 1140	273.379			
		-0.330	0.788	-0.705
025 1145	273.049			
		-0.417	0.787	-0.654
025 1150	272.632			
		-0.458	0.786	-0.632
025 1155	272.174			
		-0.528	0.784	-0.598
025 1200	271.646			
		-0.598	0.782	-0.567
025 1205	271.048			
		-0.665	0.781	-0.540
025 1210	270.383			
		-0.771	0.779	-0.502
025 1215	269.611			
		-0.887	0.776	-0.467
025 1220	268.724			
		-1.041	0.773	-0.426
025 1225	267.683			
		-1.262	0.770	-0.379
025 1230	266.421			
		-1.535	0.766	-0.333
025 1235	264.886			
		-2.088	0.761	-0.267
025 1240	262.798			
		-3.706	0.752	-0.169
025 1245	259.092			

Table 6: Back-of-the-Envelope Calculations of Required Densities

L Shell	Constant Magnetospheric Density (cm^{-3})	Slab Ionospheric Density (cm^{-3})
6.0	24.7	4.50×10^{9}
7.5	4.14	1.90×10^{9}
9.0	0.962	undefined

Table 7: Parameter Sets for the Non-Rotational Model

β_o ($sec^2 - kg^{-1} - R_U^{-2}$)	n_o (cm^{-3})
4.0×10^{34}	4.4040904×10^{7}
4.2×10^{34}	1.0547085×10^{8}
4.4×10^{34}	2.5253202×10^{8}
4.6×10^{34}	6.0454701×10^{8}
4.8×10^{34}	1.4470810×10^{9}
5.0×10^{34}	3.4635095×10^{9}
5.2×10^{34}	8.2892150×10^{9}
5.4×10^{34}	1.9837587×10^{10}
5.6×10^{34}	4.7473365×10^{10}
5.8×10^{34}	1.1360571×10^{11}
6.0×10^{34}	2.7185689×10^{11}

Table 8: Parameter Sets for the Spin-Aligned Model

$\beta_\circ$ $(sec^2 - kg^{-1} - R_U^{-2})$	$r_\circ$ (R_U)	$n_\circ$ (cm^{-3})
4.0×10^{34}	1.006477	8.2891700×10^{5}
4.2×10^{34}	1.012457	1.4502450×10^{6}
4.4×10^{34}	1.002985	3.7174750×10^{6}
4.6×10^{34}	1.012396	5.8676420×10^{6}
4.8×10^{34}	1.005042	1.4460867×10^{7}
5.0×10^{34}	1.000003	3.3927012×10^{7}
5.2×10^{34}	1.006212	5.7110336×10^{7}
5.4×10^{34}	1.003327	1.2618759×10^{8}
5.6×10^{34}	1.007953	2.1954013×10^{8}
5.8×10^{34}	1.008212	4.3737914×10^{8}
6.0×10^{34}	1.000249	1.1597521×10^{9}

Figure 1. Frequency/time spectrogram of PRA data showing radio arcs. Blue is low intensity. Red is high intensity. White is where the color scale, not the instrument itself, saturated.

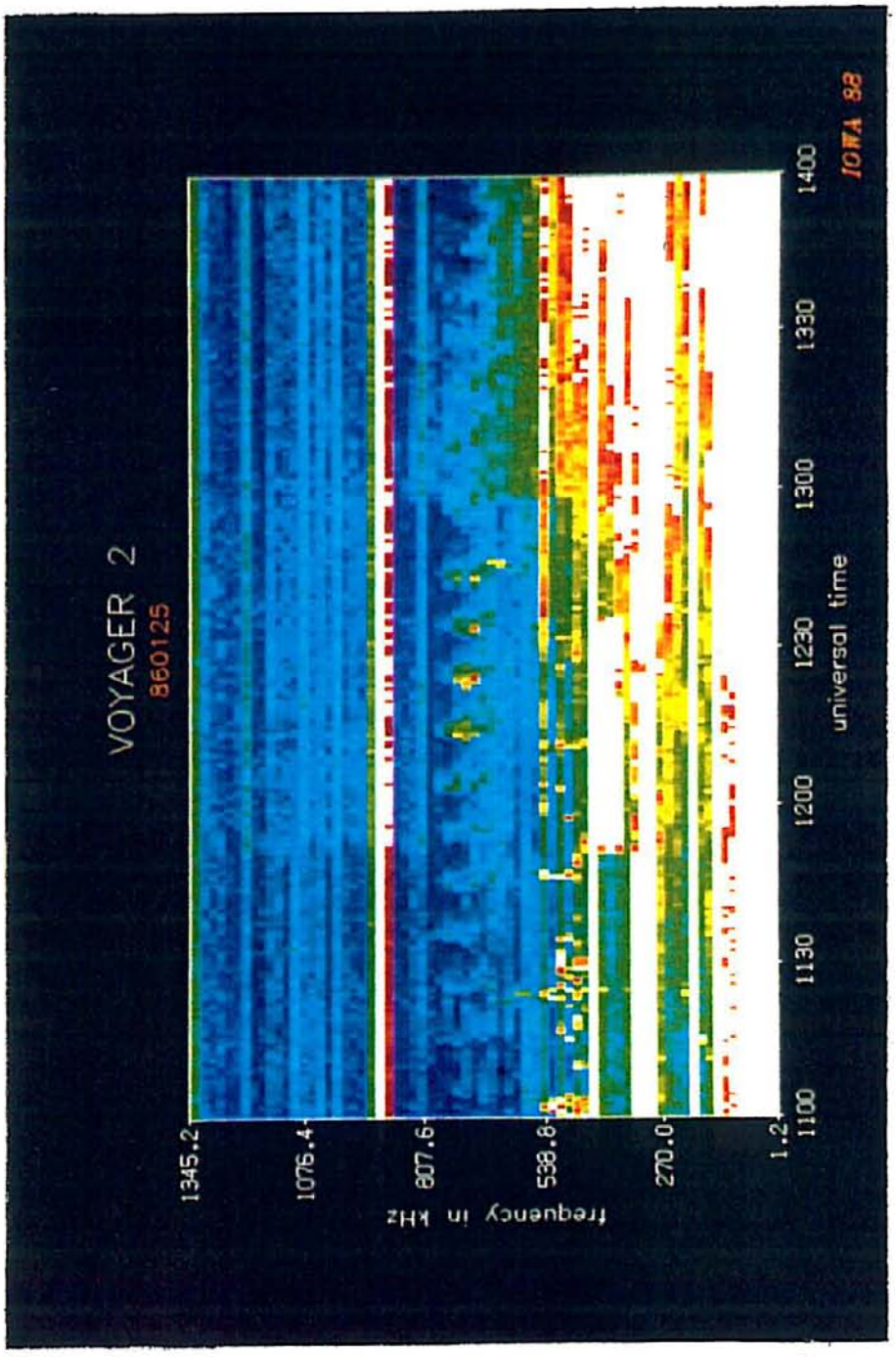
VOYAGER 2
860125
IOWA 82
frequency in kHz
1345.2
1076.4
807.6
538.8
270.0
1.2
1100
1130
1200
1230
1300
1330
1400
universal time

Figure 2. Illustration of moving conductor in a magnetized plasma.

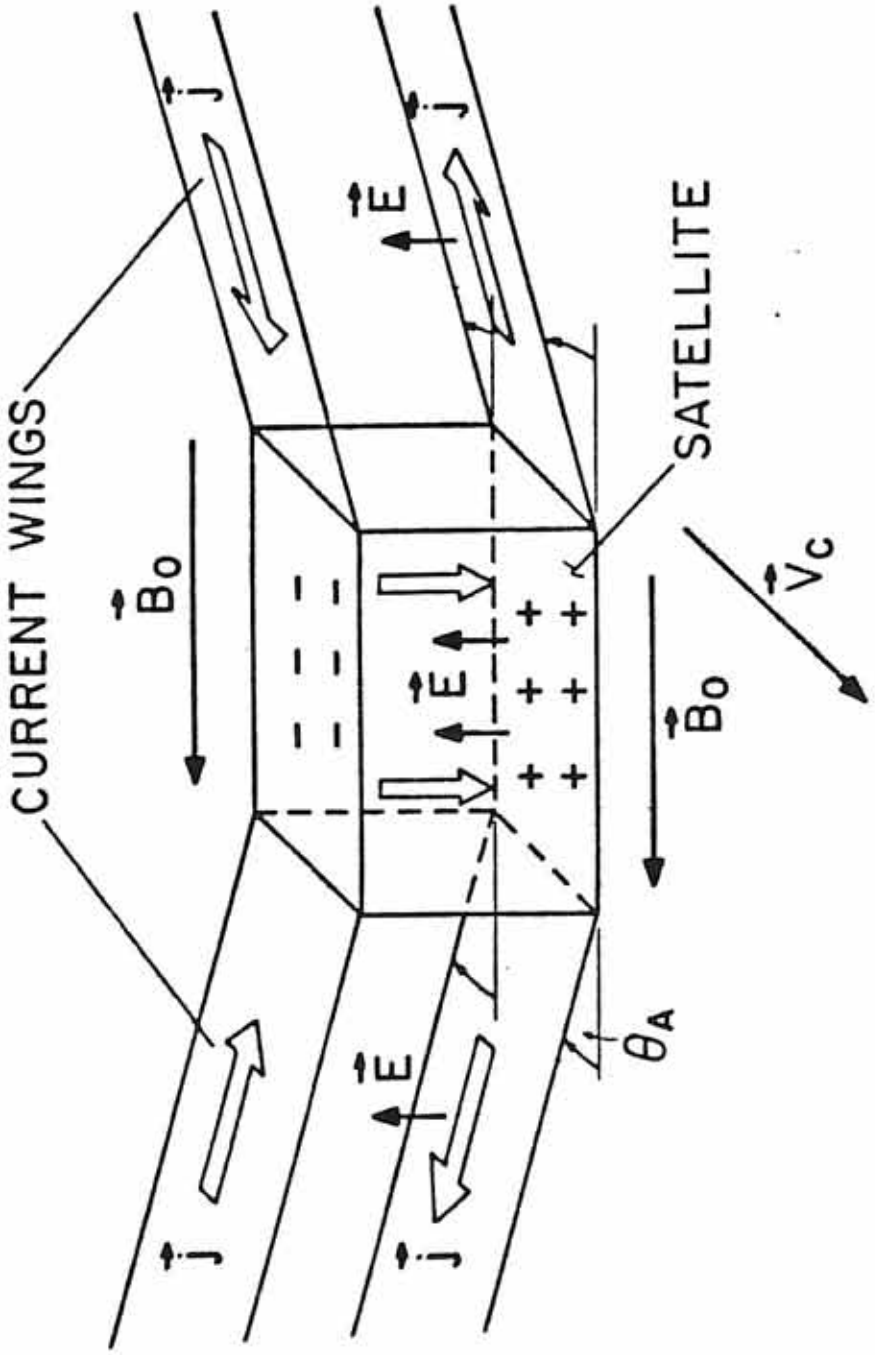
CURRENT WINGS
SATELLITE
$\vec{B}_o$
$\vec{B}_o$
$\vec{V}_c$
$\vec{E}$
$\vec{E}$
$\vec{E}$
$\vec{j}$
$\vec{j}$
$\vec{j}$
$\vec{j}$
θ_A

Figure 3. Geometric relationship among important vectors.

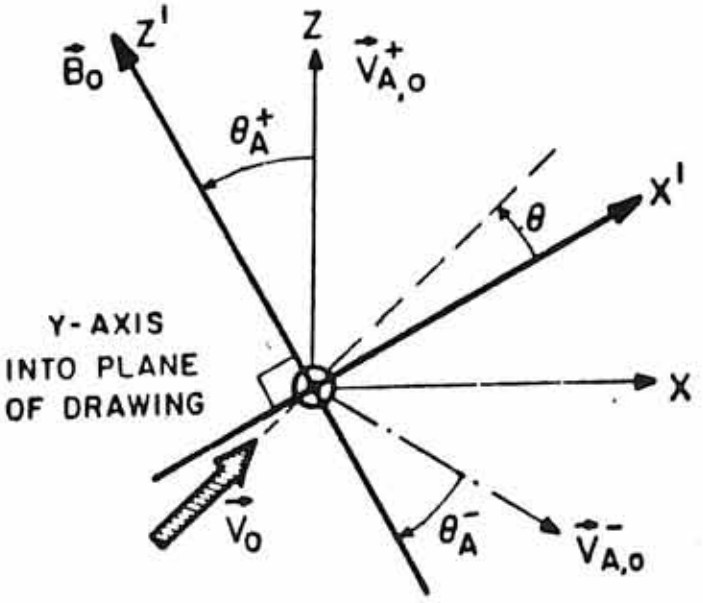
$\vec{B}_o$
Z'
Z
$\vec{V}_{A,o}^{+}$
θ_A^+
θ
X'
Y-AXIS
INTO PLANE
OF DRAWING
X
$\vec{V}_o$
θ_A^-
$\vec{V}_{A,o}^{-}$

Figure 4. Cartoon of Alfvén waves at Jupiter.

a. L shell projection of Alfvén waves

b. 3D diagram of Alfvén wave pattern

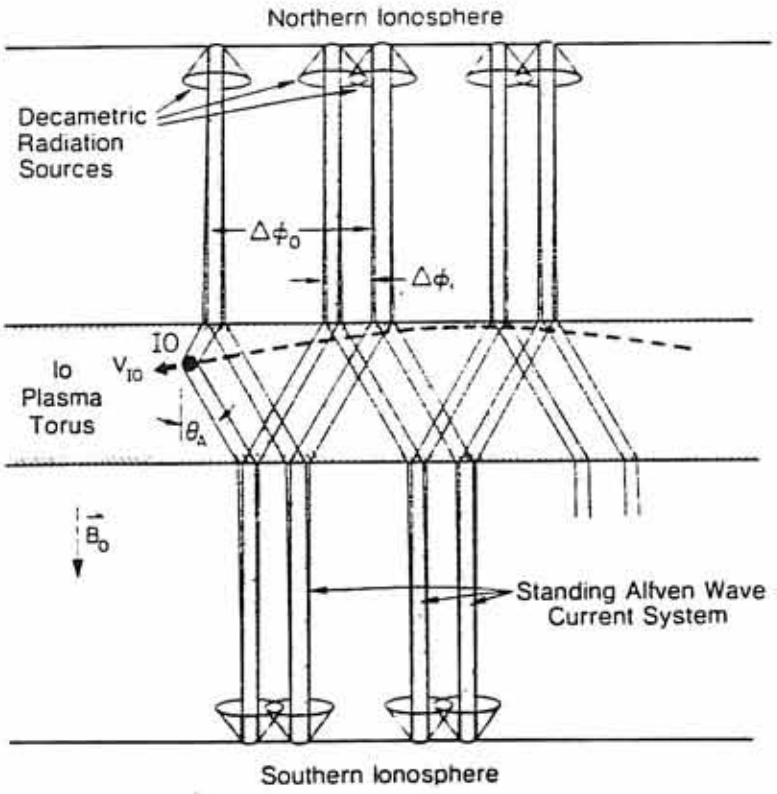
Northern Ionosphere
Decametric
Radiation
Sources
$\Delta\phi_0$
$\Delta\phi_1$
IO
Io
Plasma
Torus
V_{IO}
θ_A
$\vec{B}_0$
Standing Alfven Wave
Current System
Southern Ionosphere

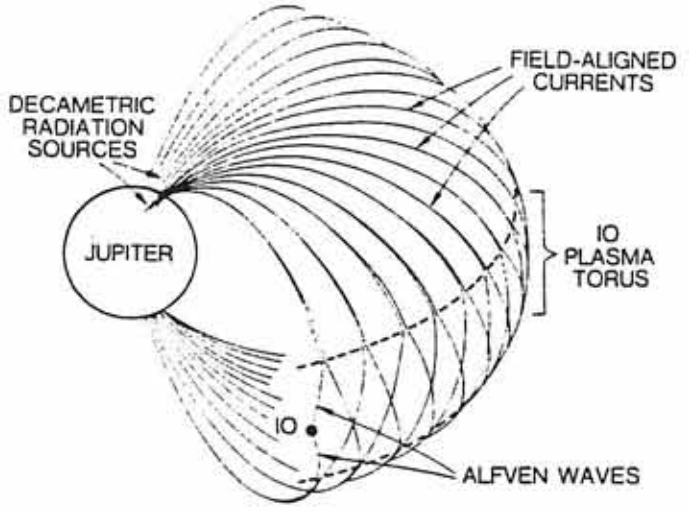
FIELD-ALIGNED
CURRENTS
DECAMETRIC
RADIATION
SOURCES
JUPITER
IO
PLASMA
TORUS
IO
ALFVEN WAVES

Figure 5. Definition of horizon and radiation cone angles. Distances are not to scale.

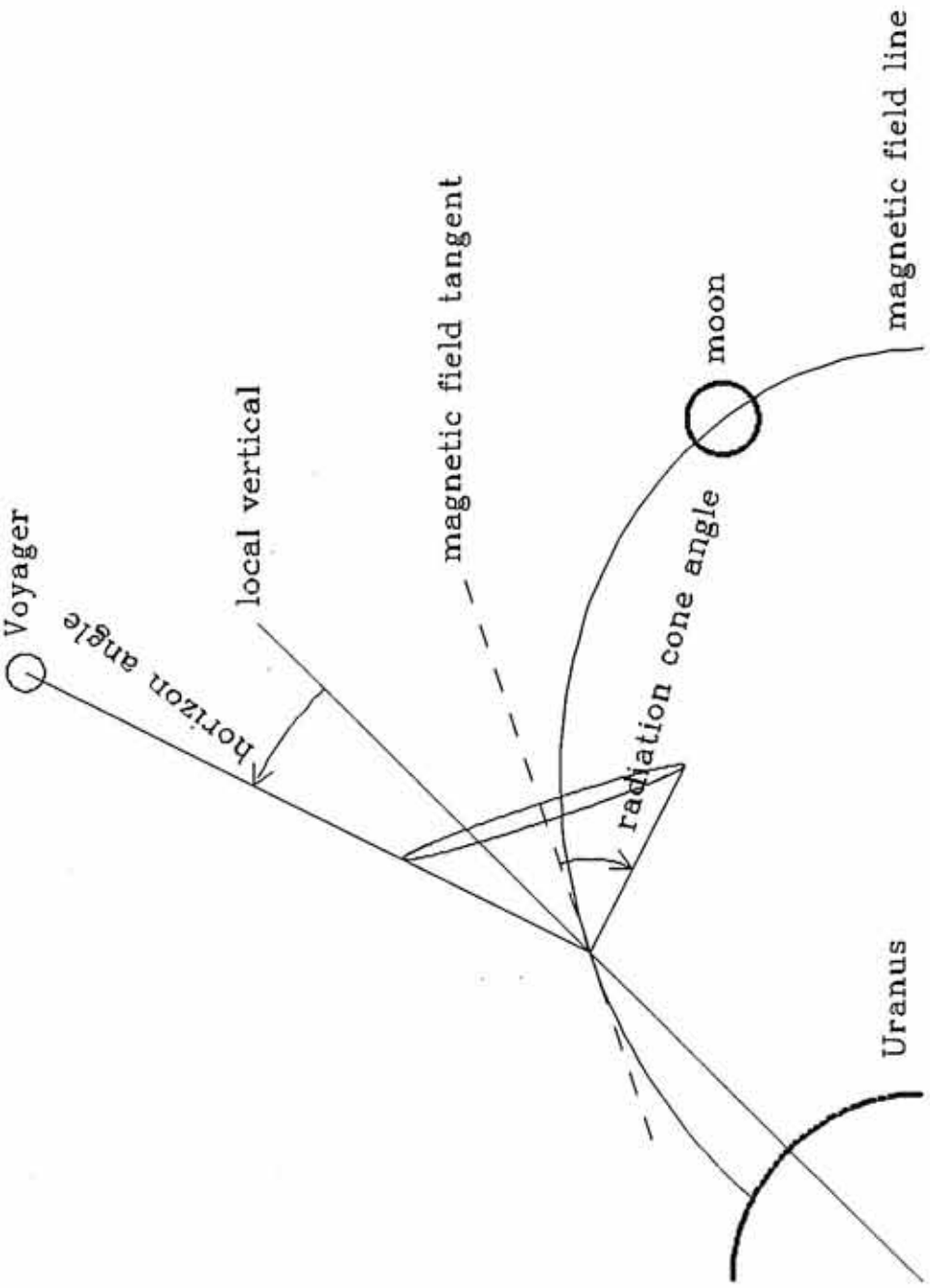
Voyager
horizon angle
local vertical
magnetic field tangent
moon
magnetic field line
radiation cone angle
Uranus

Figure 6. Illustration of magnetic latitude and longitude convention.

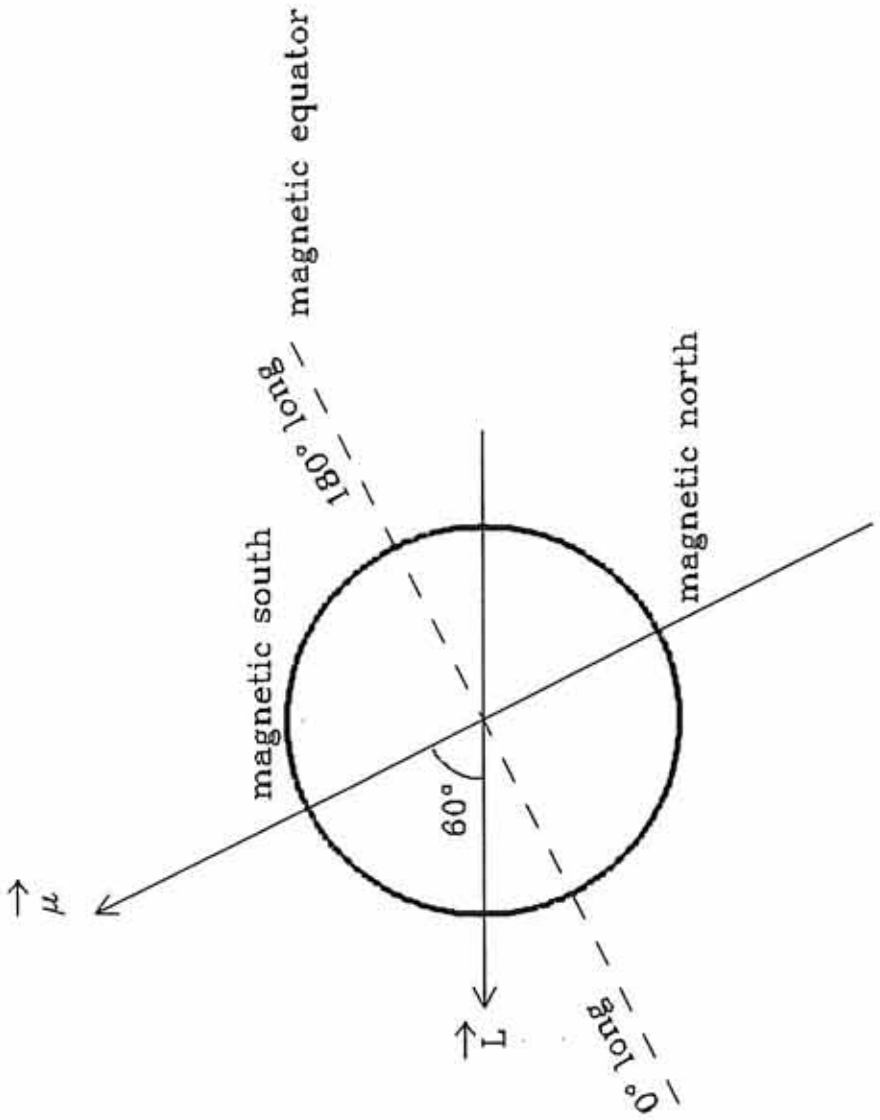
magnetic equator
180° long
magnetic north
magnetic south
60°
μ
T
0° long

Figure 7. Horizon angles to Voyager from emission point in flux tube of moon.

a. for 665 kHz radio frequency

b. for 760 kHz radio frequency

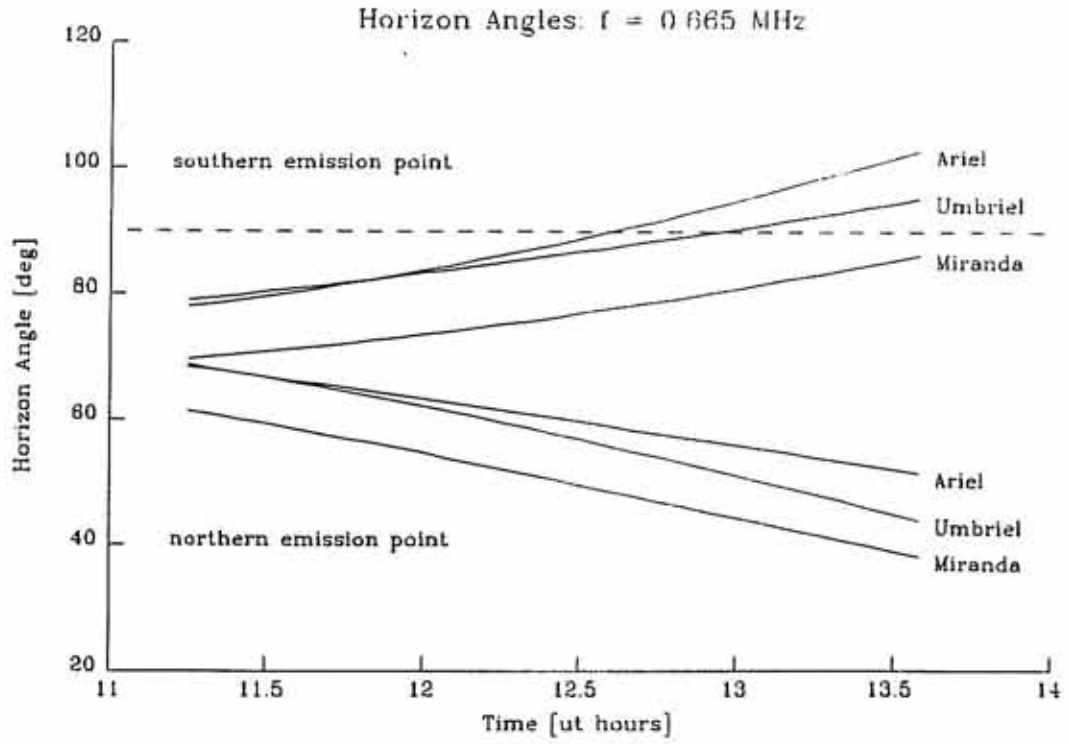
Horizon Angles: f = 0.665 MHz
120
100
80
60
40
20
Horizon Angle [deg]
southern emission point
northern emission point
Ariel
Umbriel
Miranda
Ariel
Umbriel
Miranda
11
11.5
12
12.5
13
13.5
14
Time [ut hours]

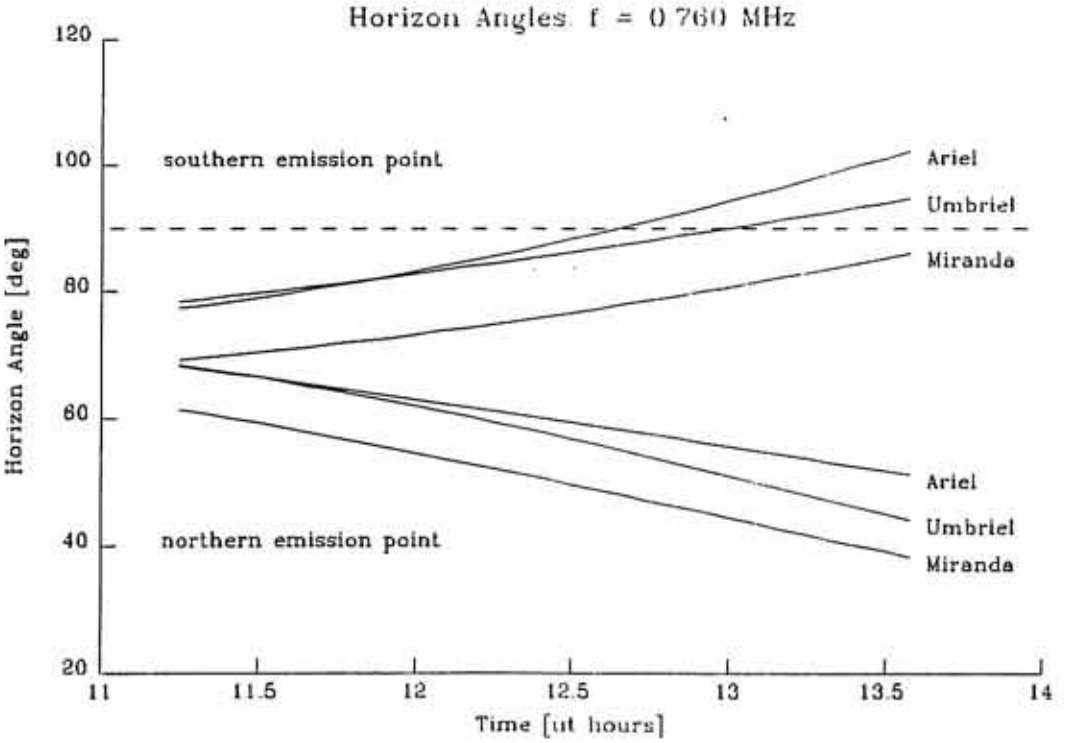
Horizon Angles: f = 0.760 MHz
120
100
80
60
40
20
Horizon Angle [deg]
southern emission point
northern emission point
Ariel
Umbriel
Miranda
Ariel
Umbriel
Miranda
11
11.5
12
12.5
13
13.5
14
Time [ut hours]

Figure 8. Radiation cone angles to Voyager from emission point in flux tube of moon.

a. for 665 kHz radio frequency

b. for 760 kHz radio frequency

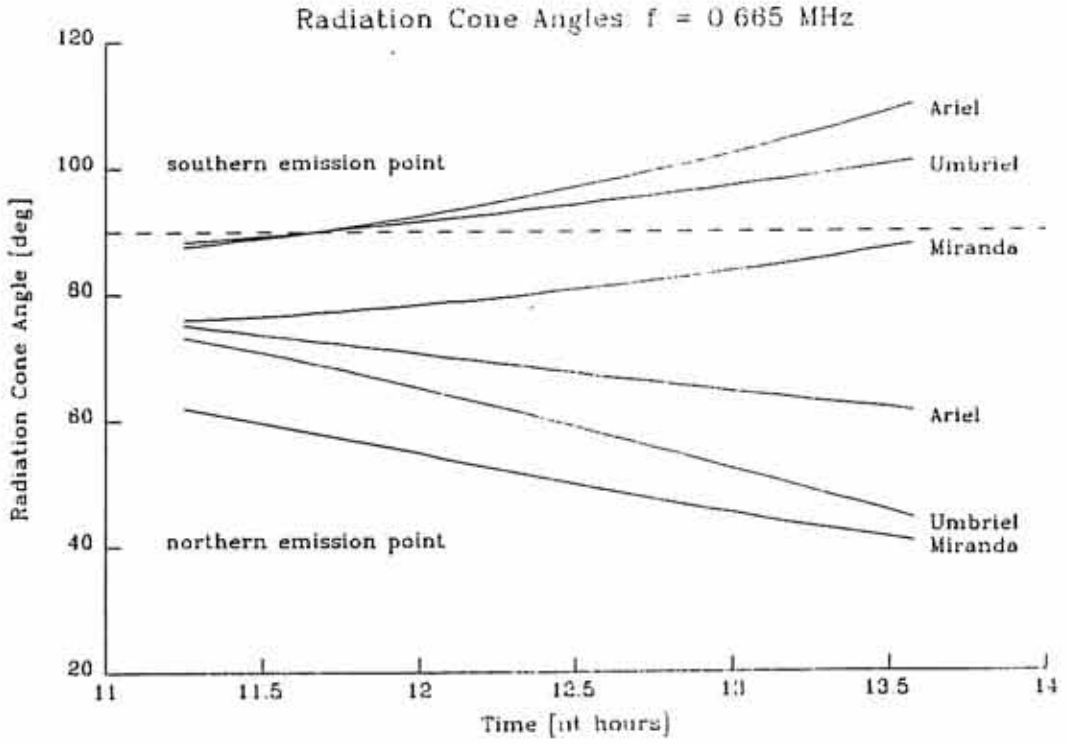
Radiation Cone Angles: f = 0.665 MHz
Radiation Cone Angle [deg]
120
100
80
60
40
20
11
11.5
12
12.5
13
13.5
14
Time [ut hours]
southern emission point
northern emission point
Ariel
Umbriel
Miranda
Ariel
Umbriel
Miranda

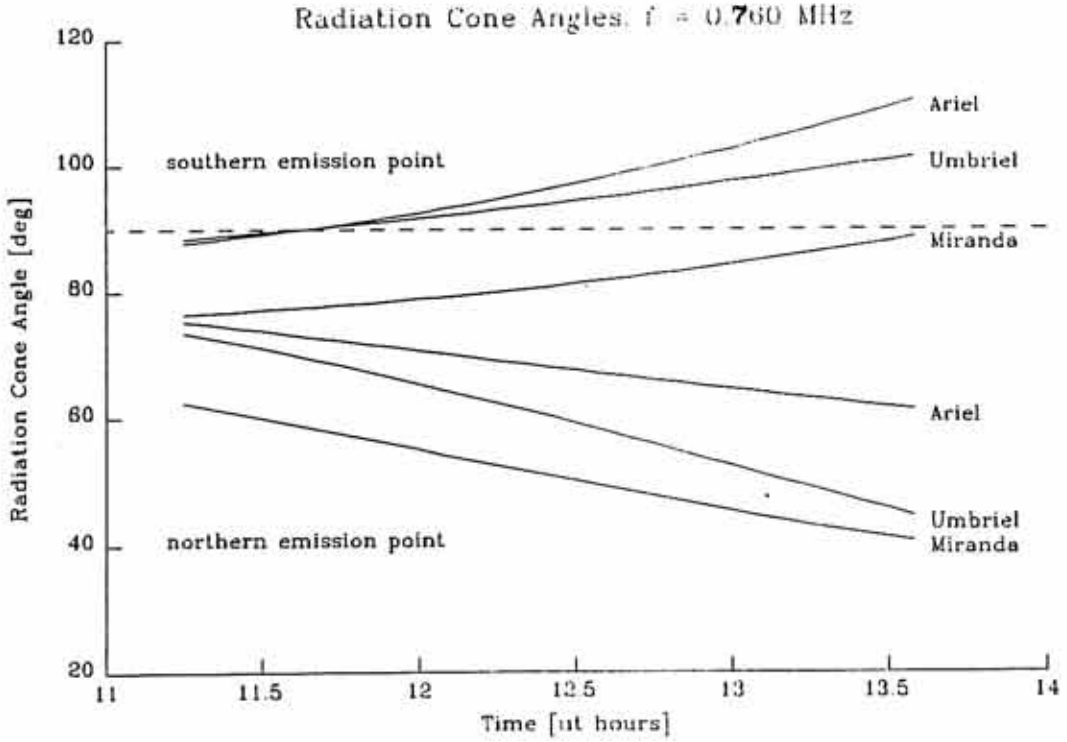
Radiation Cone Angles: f = 0.760 MHz
Radiation Cone Angle [deg]
120
100
80
60
40
20
11
11.5
12
12.5
13
13.5
14
Time [ut hours]
southern emission point
northern emission point
Ariel
Umbriel
Miranda
Ariel
Umbriel
Miranda

Figure 9. Horizon angle contours in degrees for northern emission point.

a. Alfvén waves generated by Miranda

b. Alfvén waves generated by Ariel

c. Alfvén waves generated by Umbriel

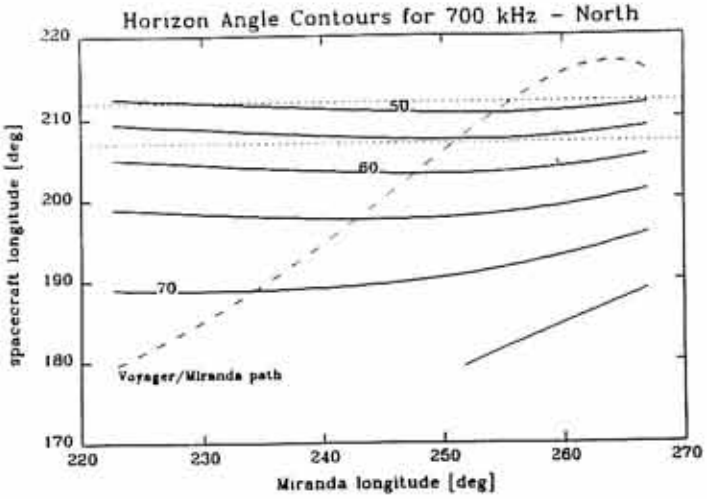
Horizon Angle Contours for 700 kHz - North
spacecraft longitude [deg]
Miranda longitude [deg]
50
60
70
Voyager/Miranda path
220
210
200
190
180
170
220
230
240
250
260
270

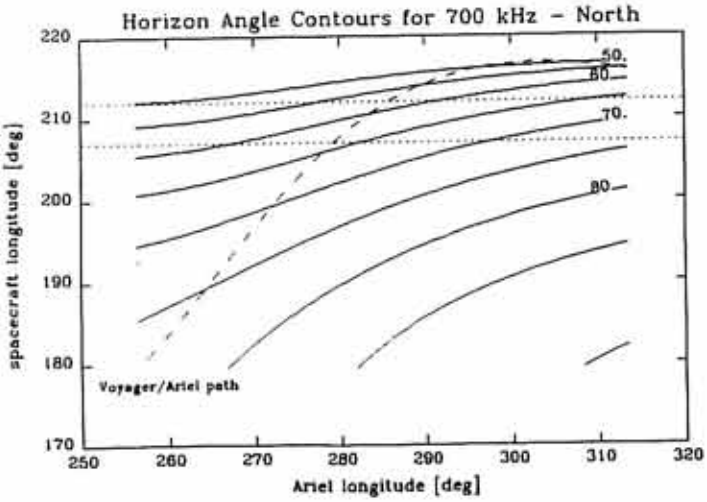
Horizon Angle Contours for 700 kHz - North
spacecraft longitude [deg]
Ariel longitude [deg]
50
60
70
80
Voyager/Ariel path
220
210
200
190
180
170
250
260
270
280
290
300
310
320

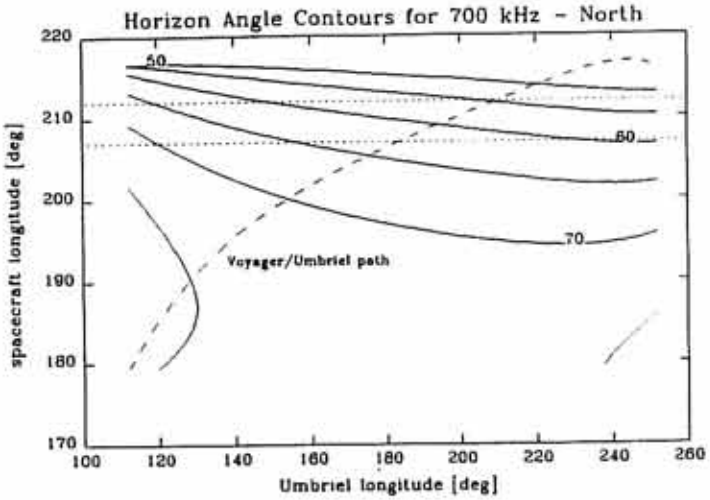
Horizon Angle Contours for 700 kHz - North
spacecraft longitude [deg]
Umbriel longitude [deg]
50
60
70
Voyager/Umbriel path
220
210
200
190
180
170
100
120
140
160
180
200
220
240
260

Figure 10. Horizon angle contours in degrees for southern emission point.

a. Alfvén waves generated by Miranda

b. Alfvén waves generated by Ariel

c. Alfvén waves generated by Umbriel

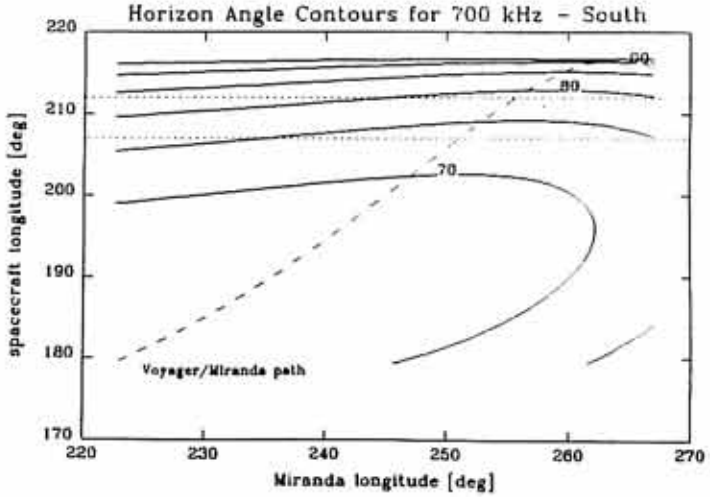
Horizon Angle Contours for 700 kHz - South
spacecraft longitude [deg]
Miranda longitude [deg]
90
80
70
Voyager/Miranda path
220
210
200
190
180
170
220
230
240
250
260
270

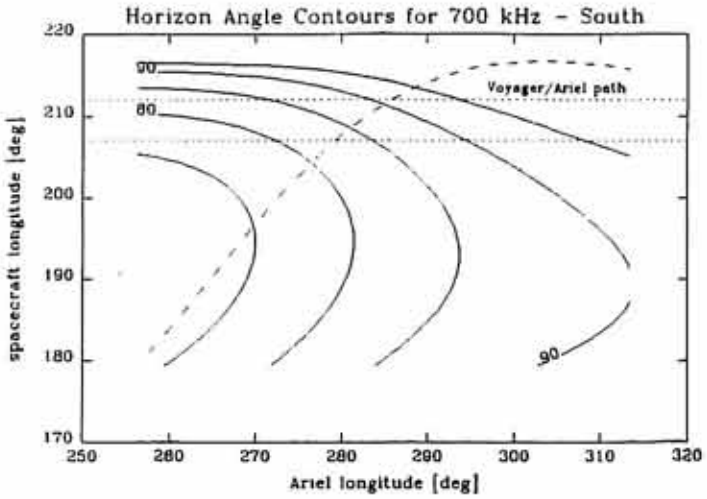
Horizon Angle Contours for 700 kHz - South
spacecraft longitude [deg]
Ariel longitude [deg]
90
80
Voyager/Ariel path
90
220
210
200
190
180
170
250
260
270
280
290
300
310
320

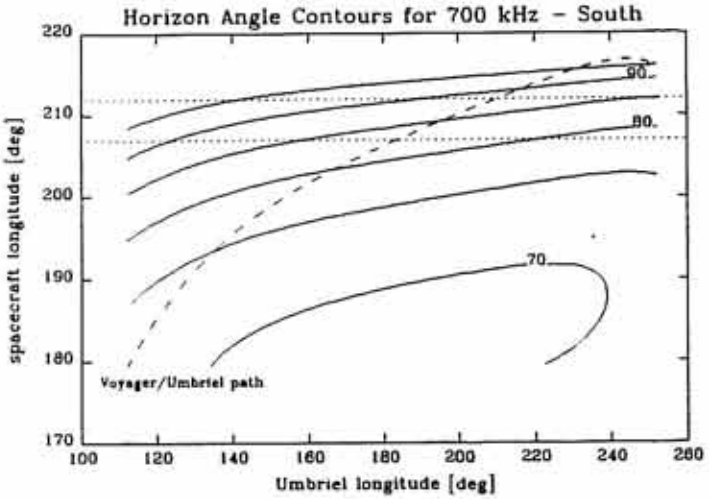
Horizon Angle Contours for 700 kHz - South
spacecraft longitude [deg]
Umbriel longitude [deg]
90
80
70
Voyager/Umbriel path
220
210
200
190
180
170
100
120
140
160
180
200
220
240
260

Figure 11. Radiation cone angle contours in degrees for northern emission point.

a. Alfvén waves generated by Miranda

b. Alfvén waves generated by Ariel

c. Alfvén waves generated by Umbriel

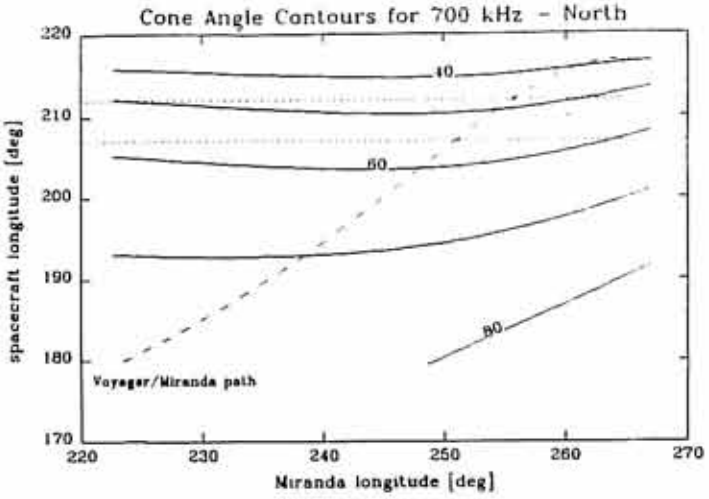
Cone Angle Contours for 700 kHz - North
spacecraft longitude [deg]
Miranda longitude [deg]
40
60
80
Voyager/Miranda path
220
210
200
190
180
170
220
230
240
250
260
270

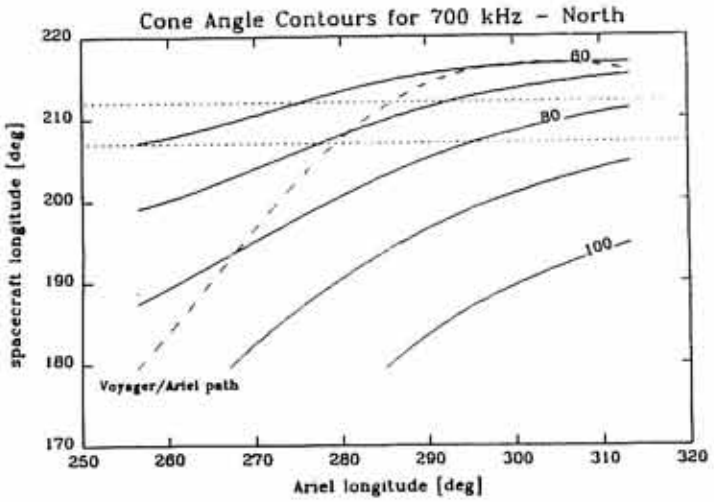
Cone Angle Contours for 700 kHz - North
spacecraft longitude [deg]
Ariel longitude [deg]
60
80
100
Voyager/Ariel path
220
210
200
190
180
170
250
260
270
280
290
300
310
320

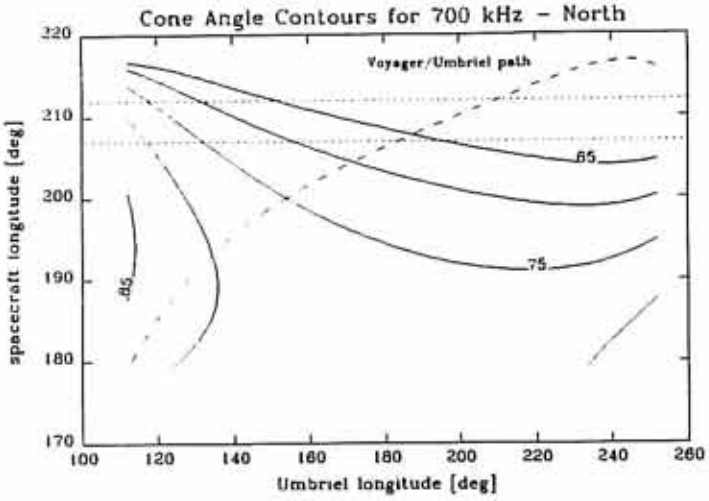
Cone Angle Contours for 700 kHz - North
spacecraft longitude [deg]
Umbriel longitude [deg]
Voyager/Umbriel path
65
75
85
220
210
200
190
180
170
100
120
140
160
180
200
220
240
260

Figure 12. Radiation cone angle contours in degrees for southern emission point.

a. Alfvén waves generated by Miranda

b. Alfvén waves generated by Ariel

c. Alfvén waves generated by Umbriel

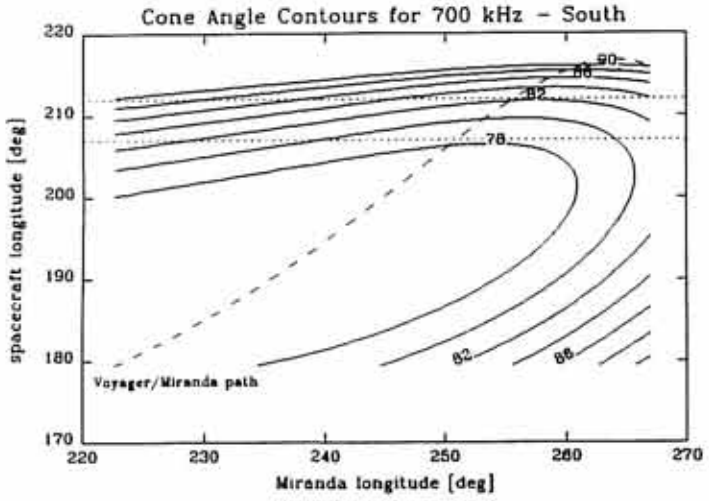
Cone Angle Contours for 700 kHz - South
90
86
82
78
82
86
Voyager/Miranda path
spacecraft longitude [deg]
Miranda longitude [deg]
220
210
200
190
180
170
220
230
240
250
260
270

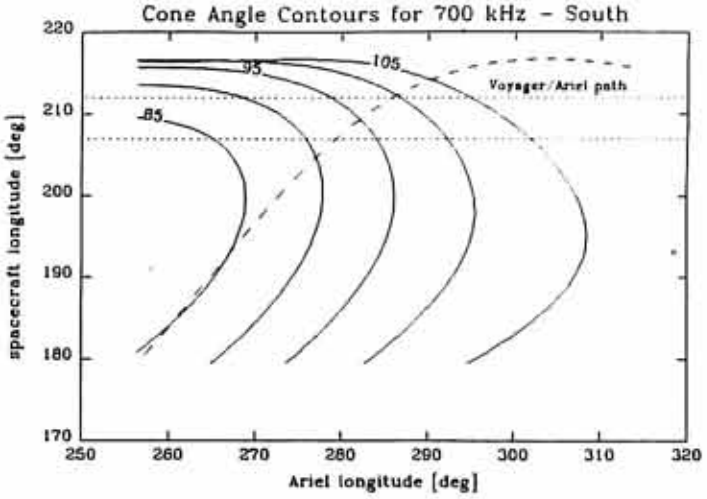
Cone Angle Contours for 700 kHz - South
95
105
85
Voyager/Ariel path
spacecraft longitude [deg]
Ariel longitude [deg]
220
210
200
190
180
170
250
260
270
280
290
300
310
320

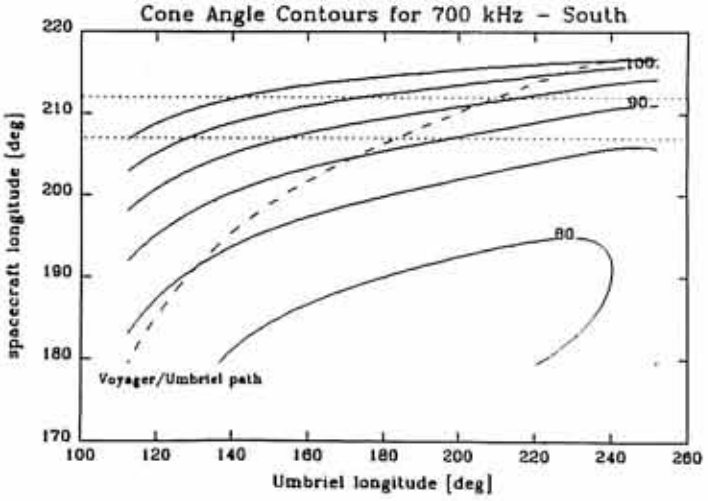
Cone Angle Contours for 700 kHz - South
100
90
80
Voyager/Umbriel path
spacecraft longitude [deg]
Umbriel longitude [deg]
220
210
200
190
180
170
100
120
140
160
180
200
220
240
260

Figure 13. RH and LH PRA averages from channels 654.0 kHz to 750.0 kHz.

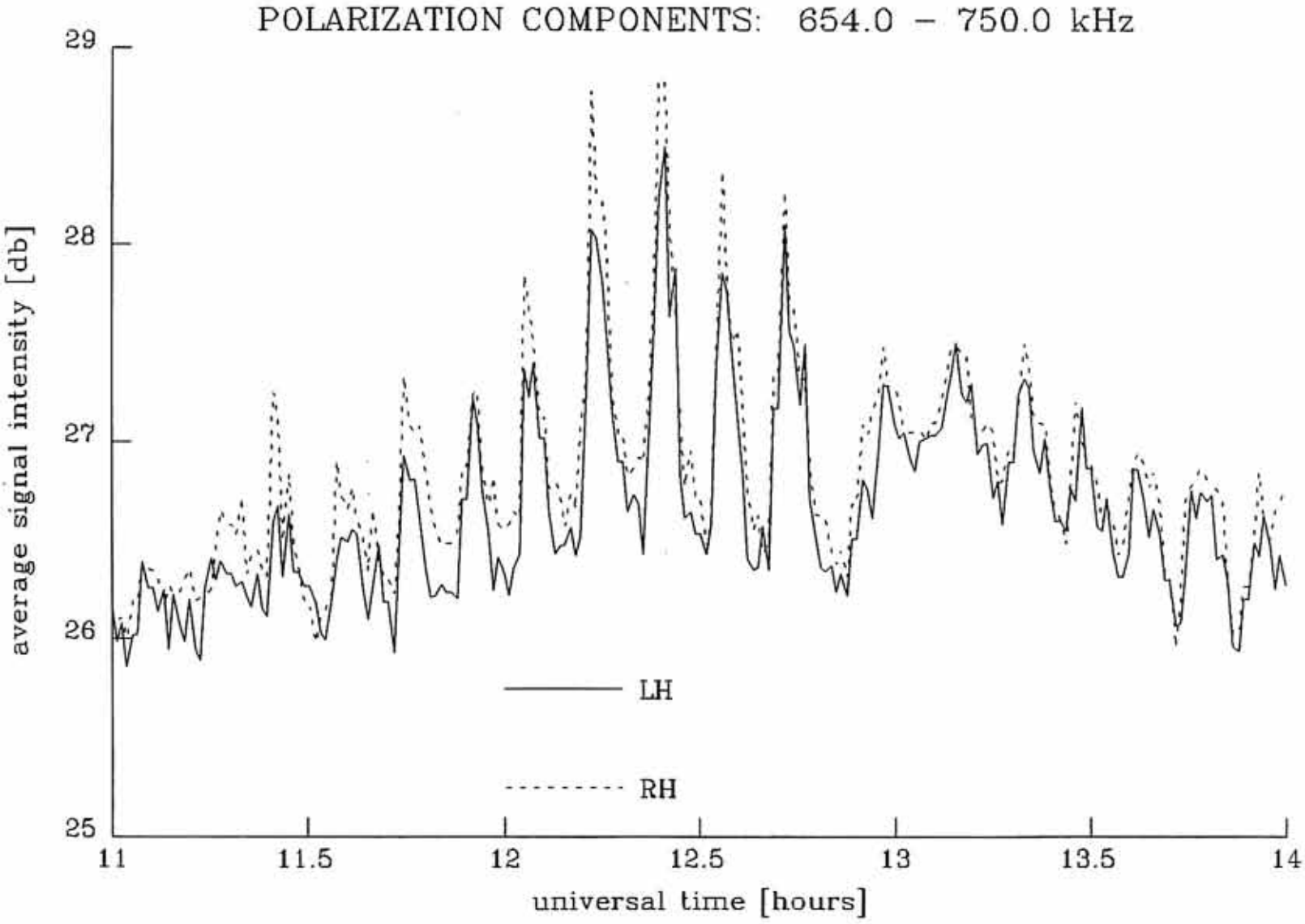
POLARIZATION COMPONENTS: 654.0 – 750.0 kHz
average signal intensity [db]
29
28
27
26
25
LH
RH
11
11.5
12
12.5
13
13.5
14
universal time [hours]

Figure 14. Cartoon of satellite motion and Alfvén image motion.

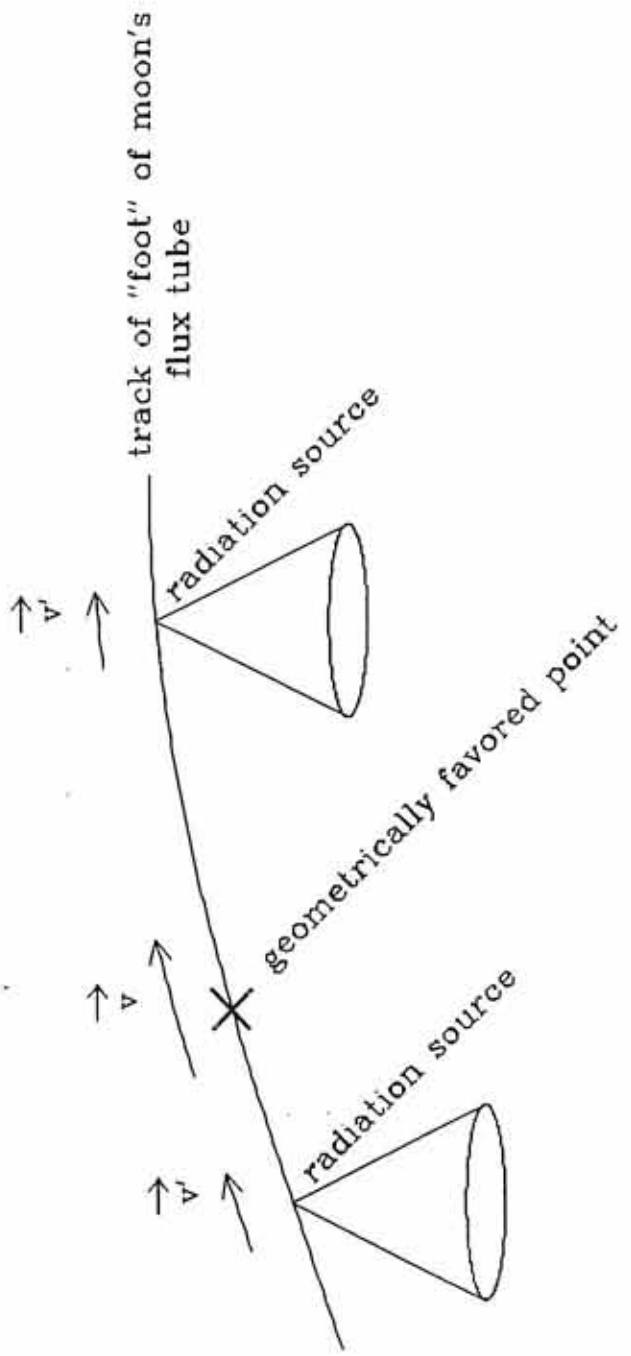
track of "foot" of moon's flux tube
radiation source
v'
geometrically favored point
v
radiation source
v'

Figure 15. Fit to density data for non-rotational model.

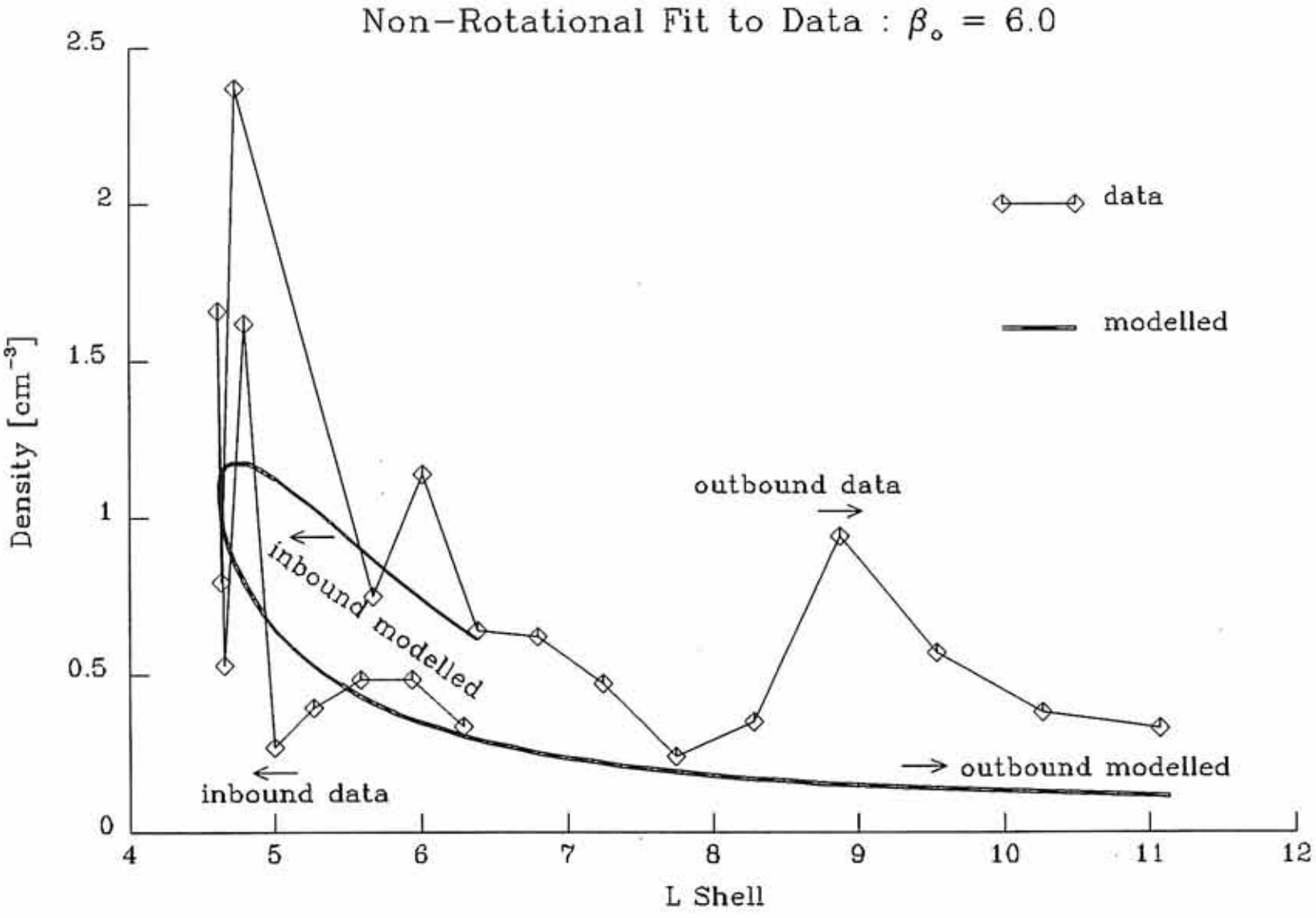
Non−Rotational Fit to Data : β_o = 6.0
Density [cm^{-3}]
2.5
2
1.5
1
0.5
0
4
5
6
7
8
9
10
11
12
L Shell
data
modelled
outbound data
inbound modelled
outbound modelled
inbound data

Figure 16. Alfvén period as a function of latitude in the non-rotational model.

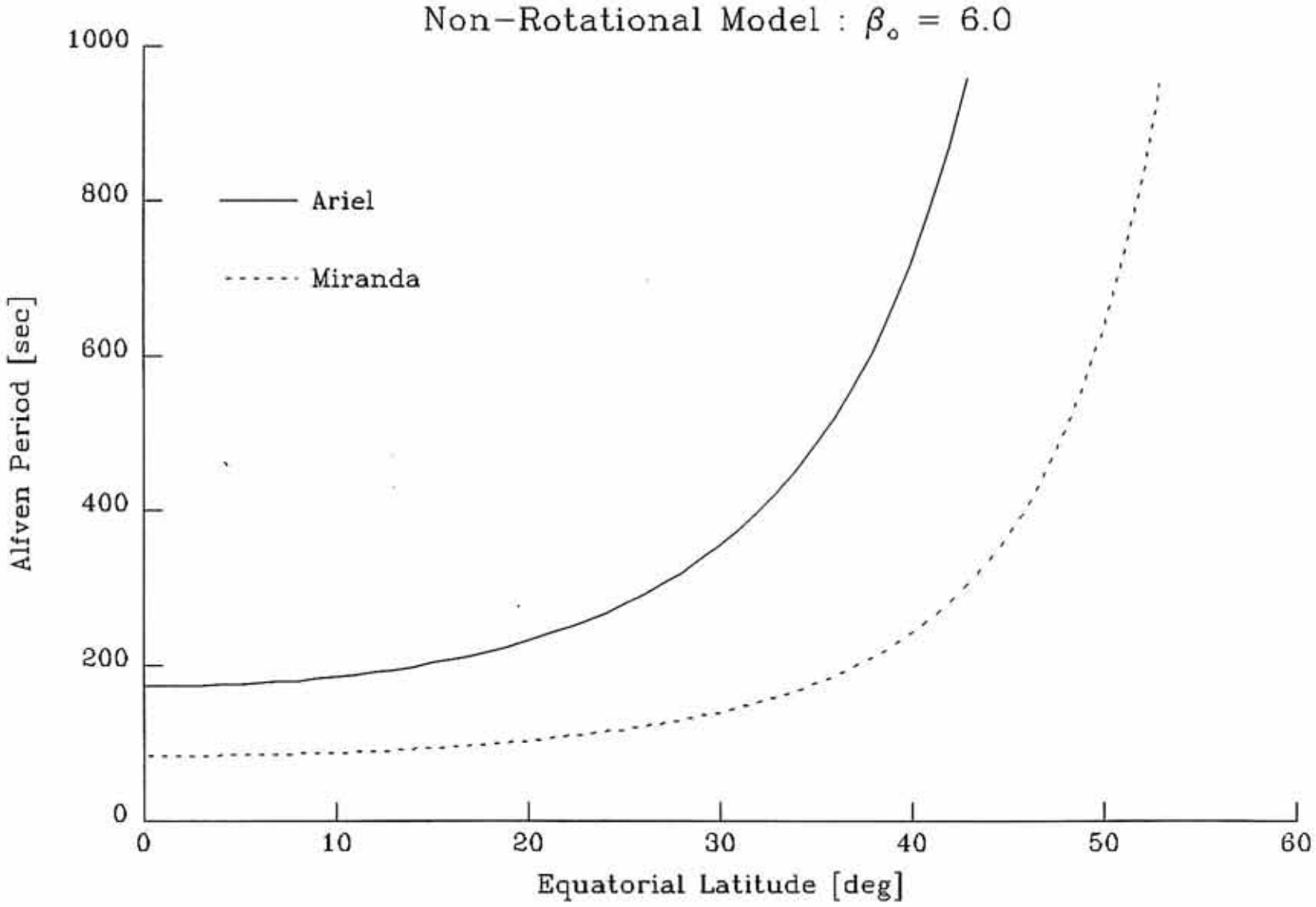
Non−Rotational Model : β_o = 6.0
Ariel
Miranda
Alfven Period [sec]
1000
800
600
400
200
0
0
10
20
30
40
50
60
Equatorial Latitude [deg]

Figure 17. Period as a function of ionospheric density for the non-rotational model.

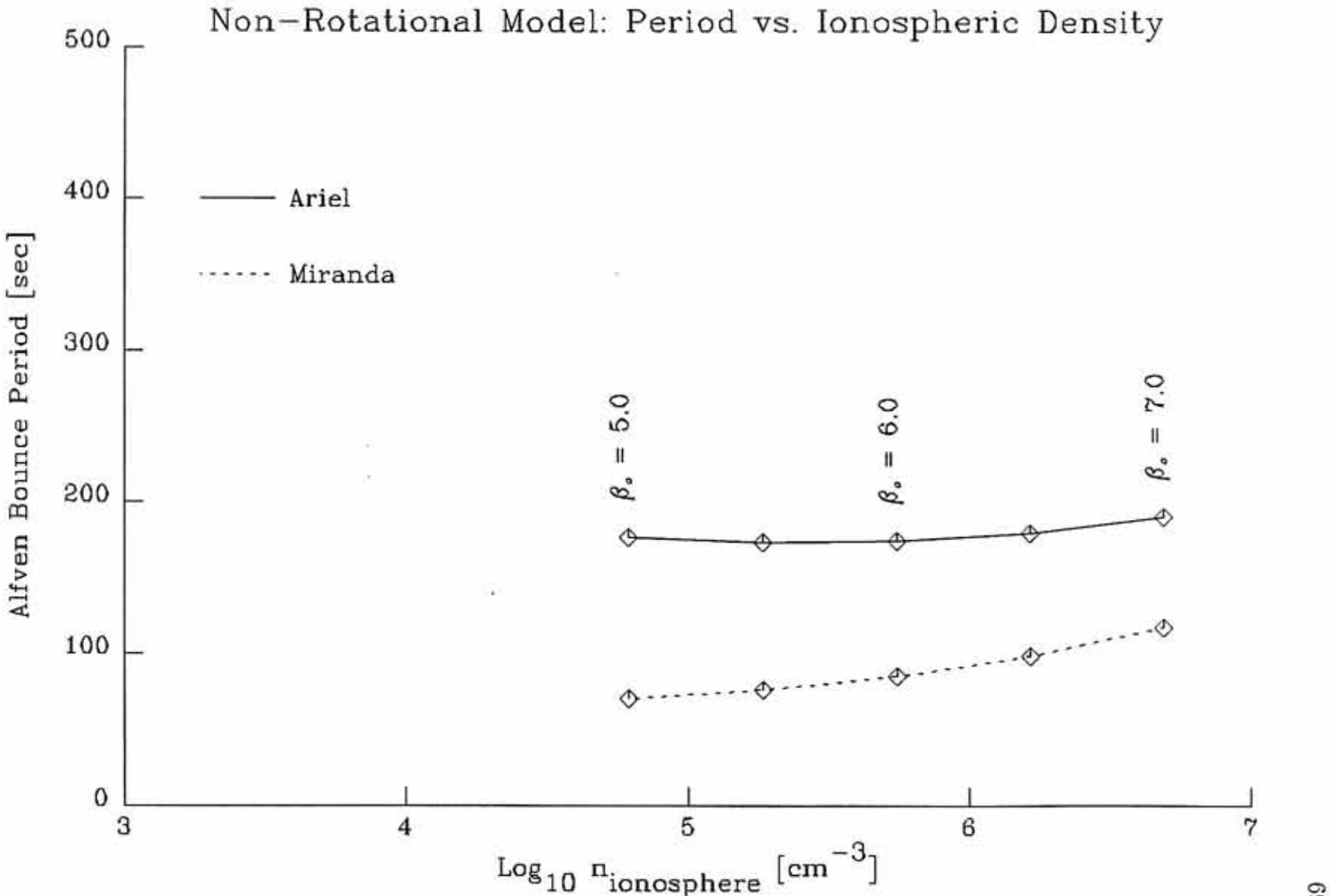
Non−Rotational Model: Period vs. Ionospheric Density
Ariel
Miranda
$\beta_\circ$ = 5.0
$\beta_\circ$ = 6.0
$\beta_\circ$ = 7.0
Alfven Bounce Period [sec]
500
400
300
200
100
0
3
4
5
6
7
$\mathrm{Log}_{10}\ n_{\mathrm{ionosphere}}\ [\mathrm{cm}^{-3}]$

Figure 18. Three divisions to space used by the spin-aligned model.

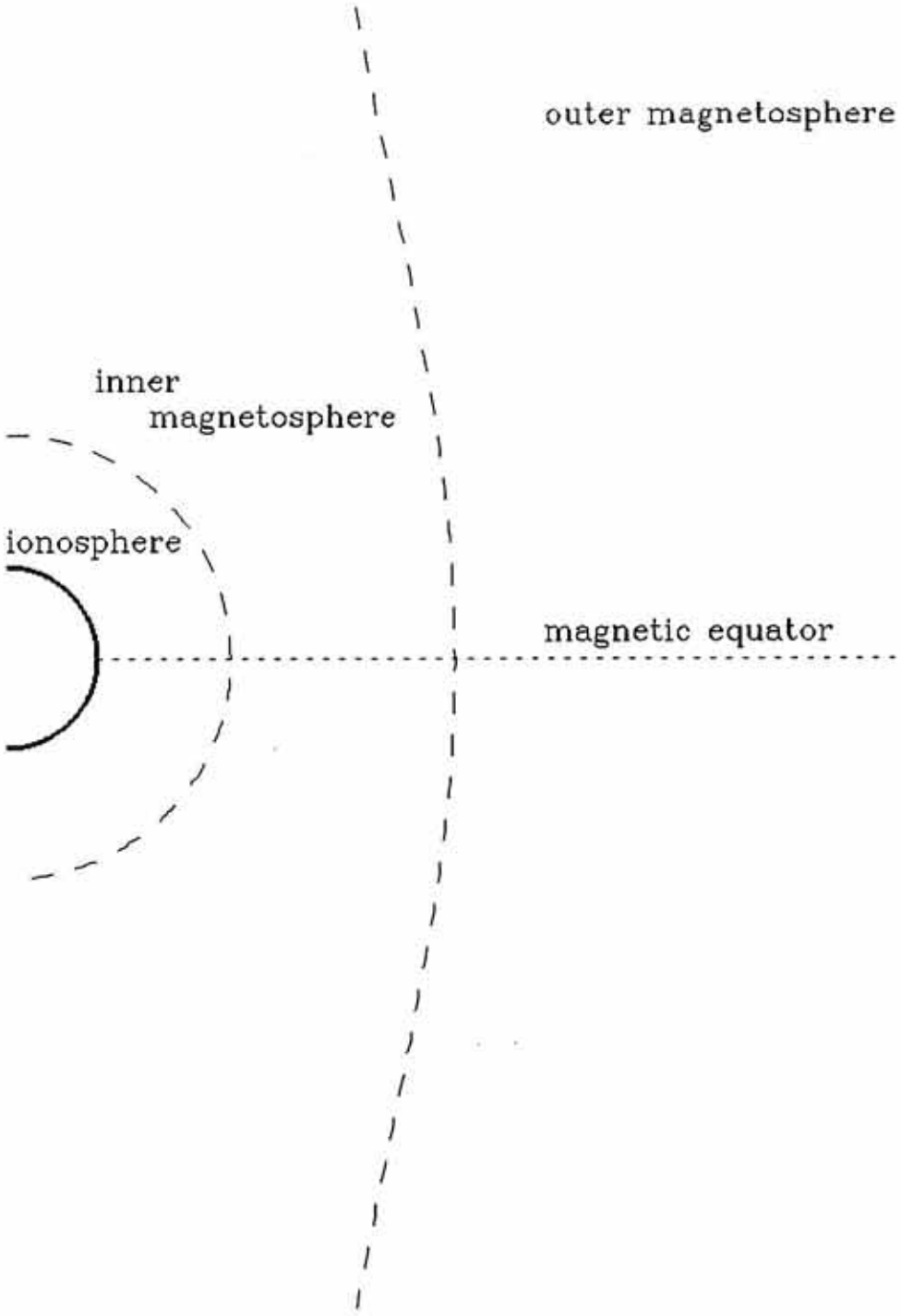
outer magnetosphere
inner
magnetosphere
ionosphere
magnetic equator

Figure 19. Potential energy along a magnetic field line, illustrating a centrifugal well.

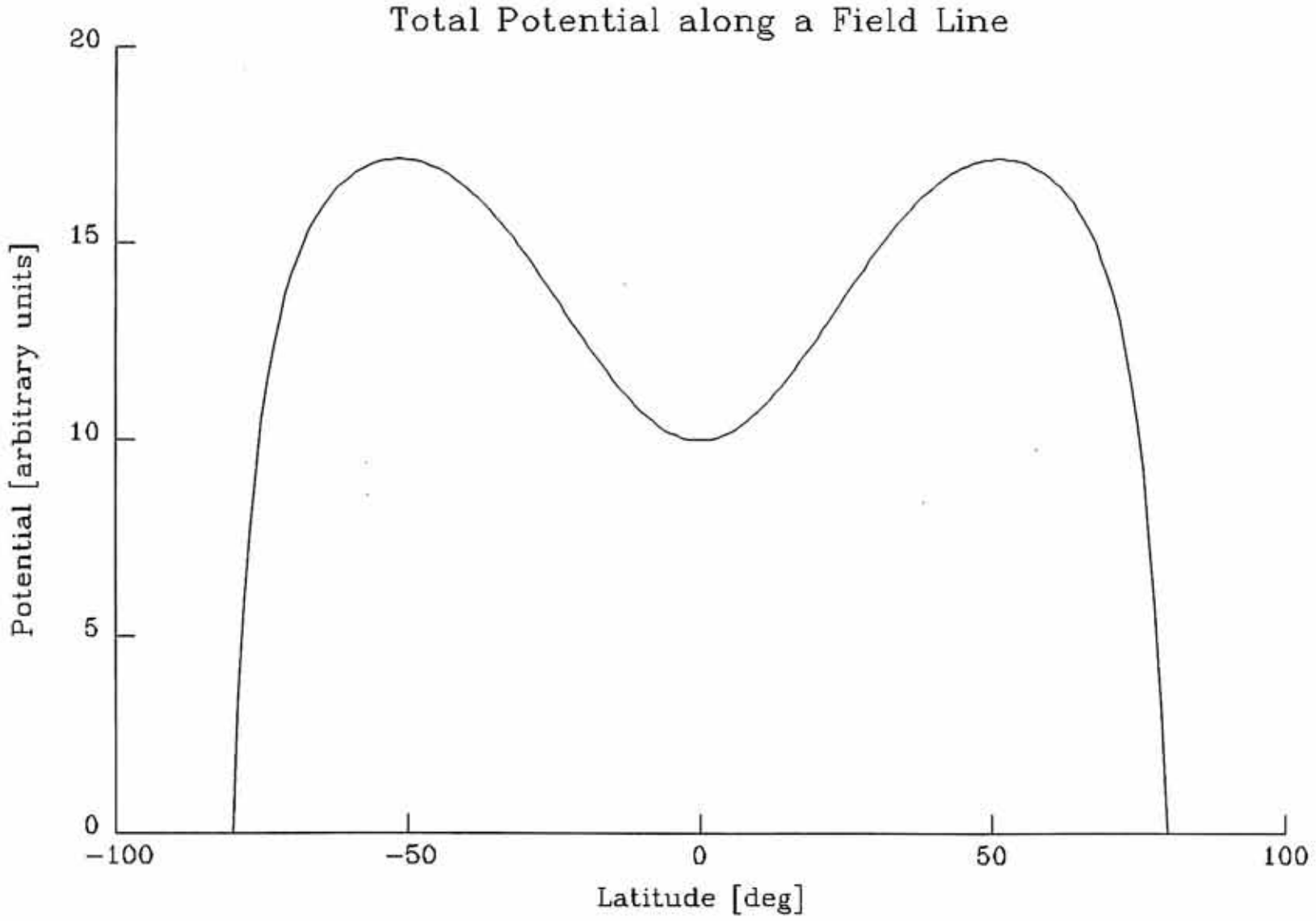
Total Potential along a Field Line
Potential [arbitrary units]
20
15
10
5
0
−100
−50
0
50
100
Latitude [deg]

Figure 20. Fit to density data for the spin-aligned model.

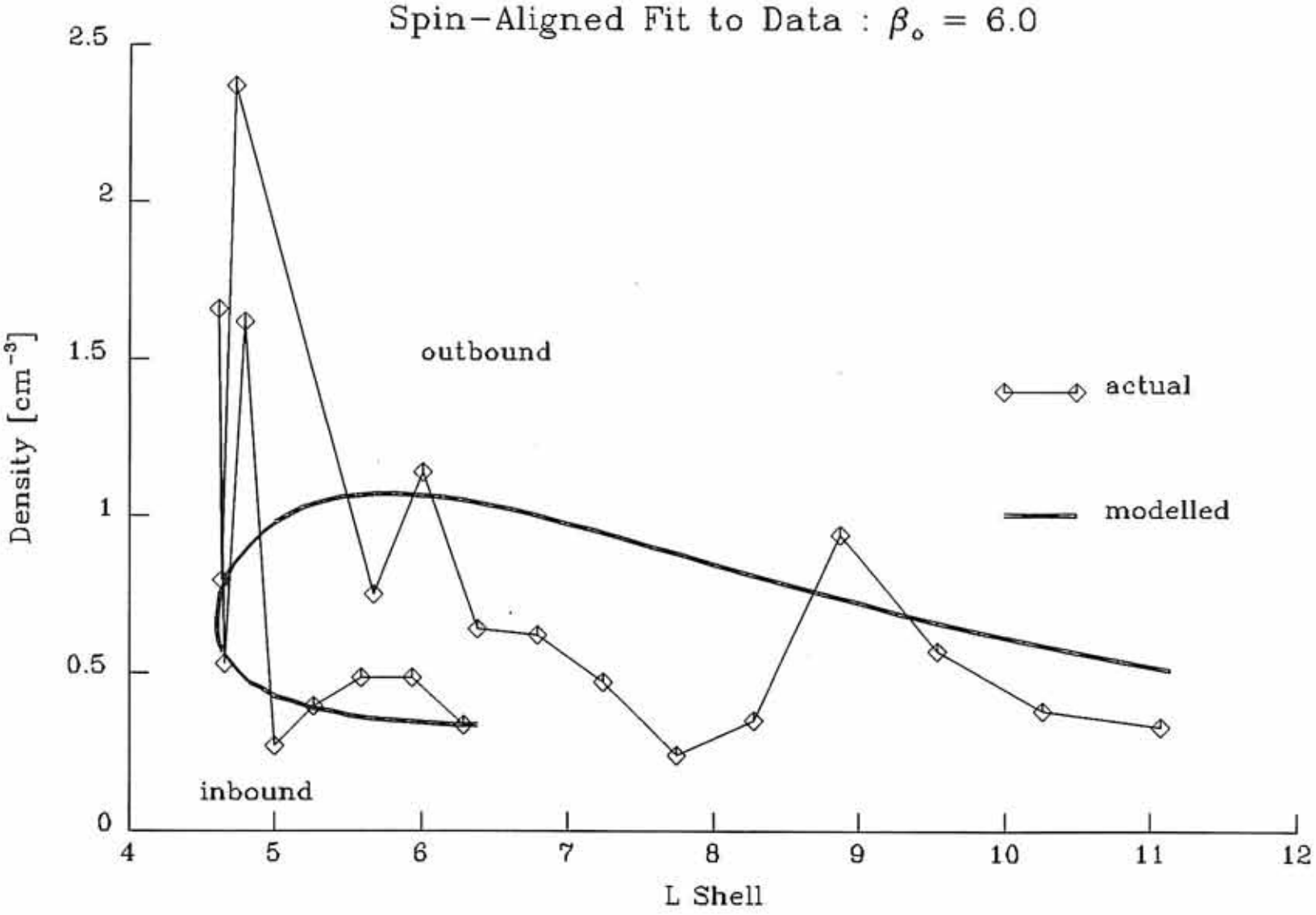
Spin−Aligned Fit to Data : β_o = 6.0
Density [cm^{-3}]
2.5
2
1.5
1
0.5
0
outbound
inbound
actual
modelled
4
5
6
7
8
9
10
11
12
L Shell

Figure 21. Alfvén period as a function of latitude in the spin-aligned model.

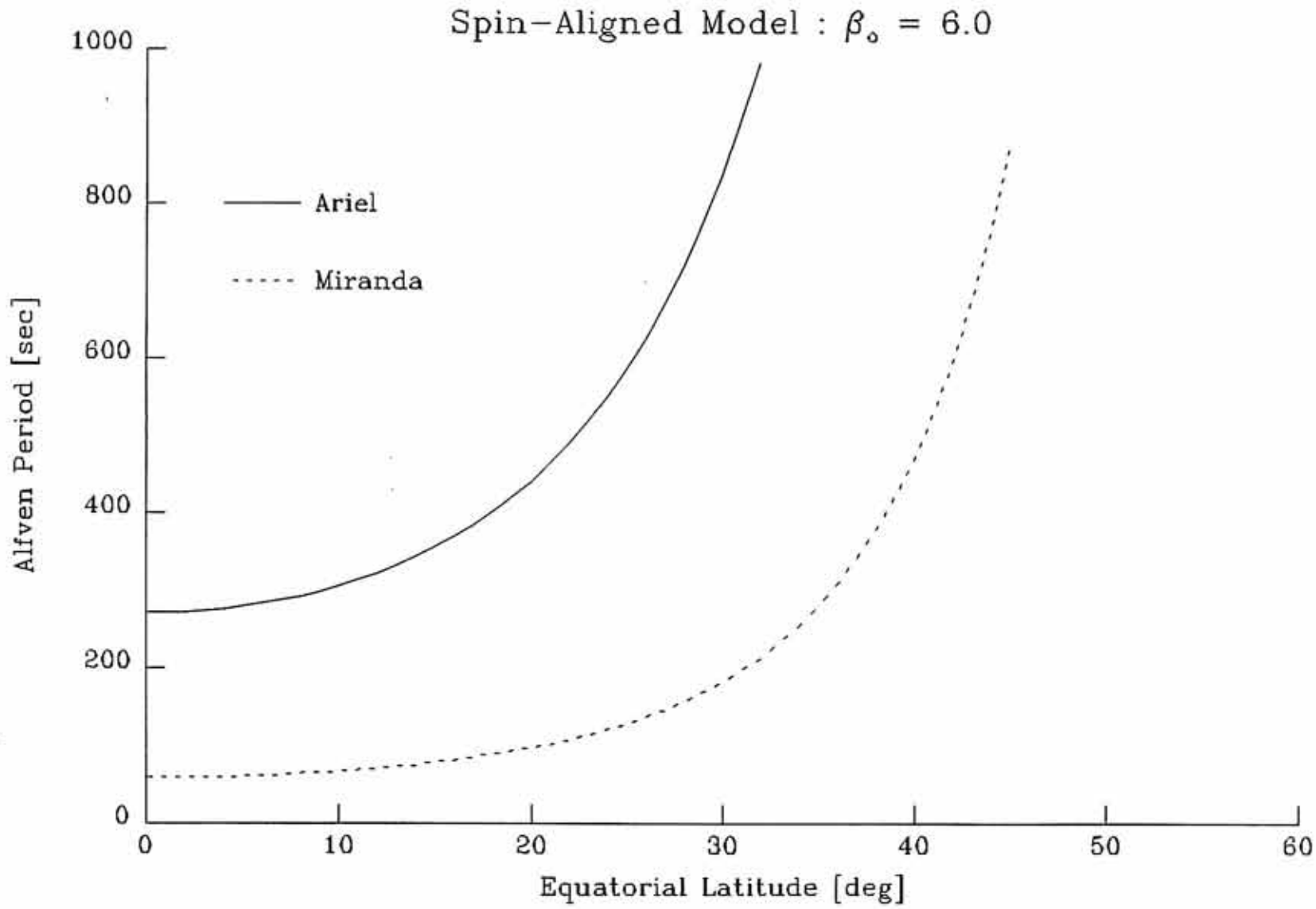
Spin−Aligned Model : β_o = 6.0
1000
800
600
400
200
0
Alfven Period [sec]
Ariel
Miranda
0
10
20
30
40
50
60
Equatorial Latitude [deg]

Figure 22. Period as a function of ionospheric density for the spin-aligned model.

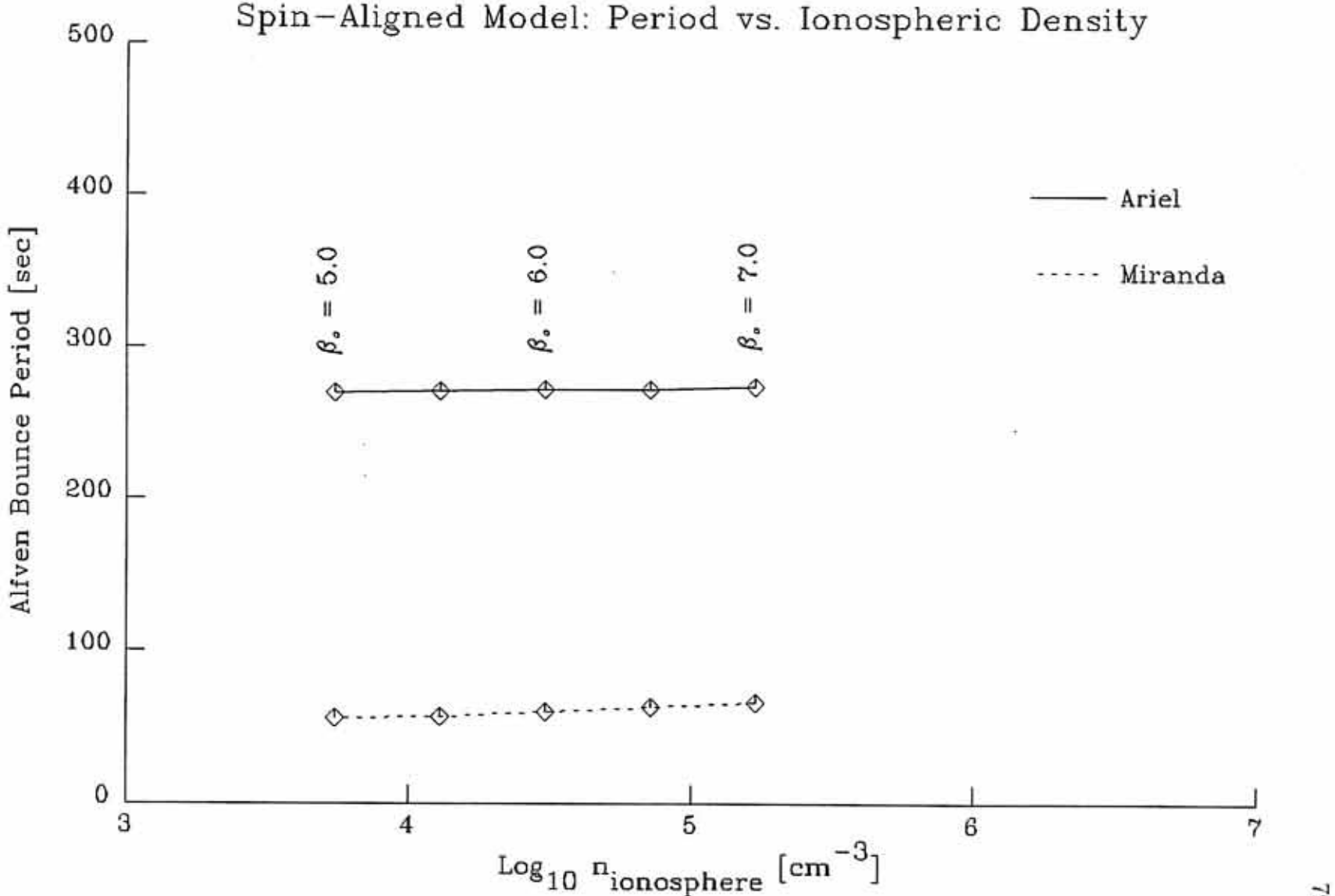
Spin−Aligned Model: Period vs. Ionospheric Density
Alfven Bounce Period [sec]
500
400
300
200
100
0
3
4
5
6
7
Log10 nionosphere [cm−3]
β° = 5.0
β° = 6.0
β° = 7.0
Ariel
Miranda

Figure 23. Near/far reflection times and minimum required time.

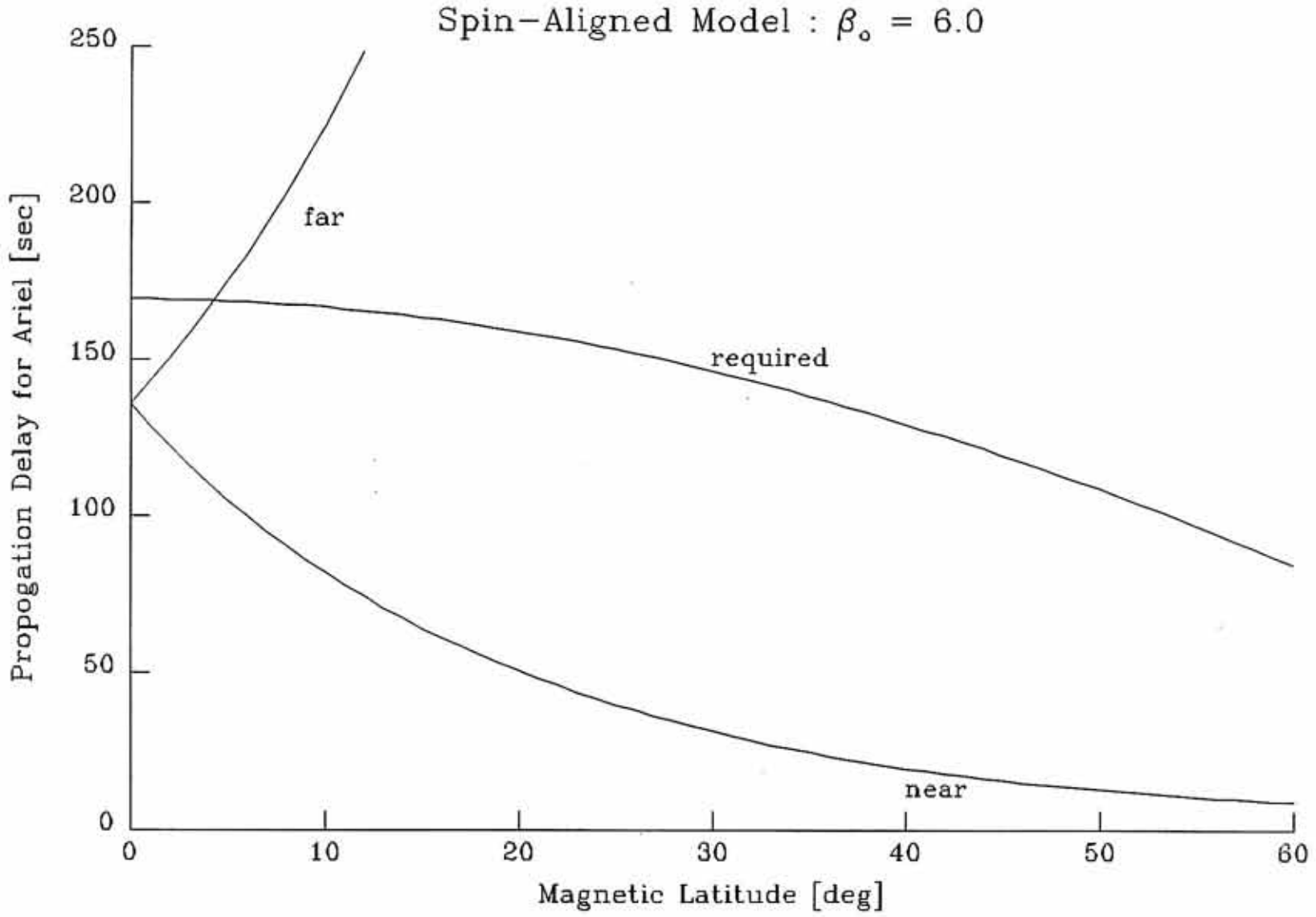
Spin−Aligned Model : β_o = 6.0
Propogation Delay for Ariel [sec]
250
200
150
100
50
0
far
required
near
0
10
20
30
40
50
60
Magnetic Latitude [deg]

Figure 24. Predicted period for the radio arcs as a function of time.

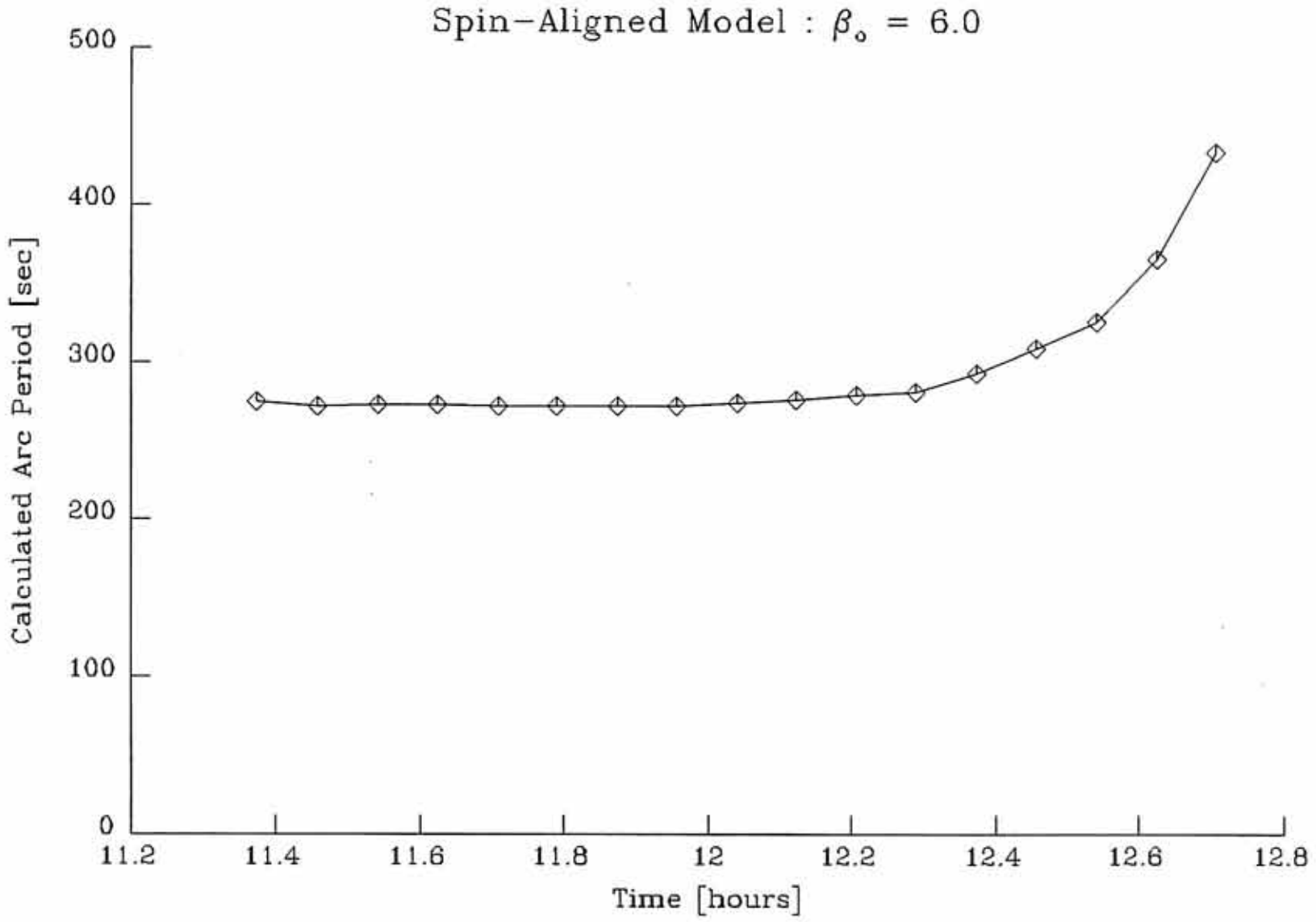
Spin−Aligned Model : β_o = 6.0
Calculated Arc Period [sec]
500
400
300
200
100
0
11.2
11.4
11.6
11.8
12
12.2
12.4
12.6
12.8
Time [hours]

REFERENCES

H. S. Bridge, J. W. Belcher, B. Coppi, A. J. Lazarus, R. L. McNutt, Jr., S. Olbert, J. D. Richardson, M. R. Sands, R. S. Selesnick, J. D. Sullivan, R. E. Hartle, K. W. Ogilvie, E. C. Sittler, Jr., F. Bagenal, R. S. Wolff, V. M. Vasyliunas, G. L. Siscoe, C. K. Goertz, A. Eviatar, "Plasma Observations Near Uranus: Initial Results from Voyager 2," *Science* **233**, 89–93, (4 July 1986).

H. S. Bridge and J. W. Belcher, communication (26 July 1986).

S. D. Drell, H. M. Foley, and M. A. Ruderman, "Drag and Propulsion of Large Satellites in the Ionosphere: An Alfvén Propulsion Engine in Space," *Journal of Geophysical Research* **70**, 3131–3145, (1 July 1965).

W. M. Farrell and W. Calvert, "The Source Location and Beaming of Broadband Bursty Radio Emissions from Uranus," submitted to *Journal of Geophysical Research*, (April 1988).

J. A. Gledhill, "Magnetosphere of Jupiter," *Nature* **214**, 155–156, (8 April 1967).

D. A. Gurnett and C. K. Goertz, "Multiple Alfvén Wave Reflections Excited by Io: Origin of the Jovian Decametric Arcs," *Journal of Geophysical Research* **86**, 717–722, (1 February 1981).

F. Herbert, B. R. Sandel, R. V. Yelle, J. B. Holberg, A. L. Broadfoot, D. E. Shemansky, S. K. Atreya, and P. N. Romani, "The Upper Atmosphere of Uranus: EUV Occultations Observed by Voyager 2," *Journal of Geophysical Research* **92**, 15093–15109, (30 December 1987).

T. W. Hill, A. J. Dessler, and F. M. Michel, "Configuration of the Jovian Magnetosphere," *Geophysical Research Letters* **1**, 3–6, (May 1974).

M. L. Kaiser, M. D. Desch, J. E. P. Connerney, "Saturn's Ionosphere: Inferred Electron Densities," *Journal of Geophysical Research* **89**, 2371–2376, (1 April 1984).

Y. Leblanc, M. G. Aubier, A. Ortega-Molina, and A. Lecacheux, "Overview of the Uranian Radio Emissions: Polarization and Constraints on Source Locations," *Journal of Geophysical Research* **92**, 15125–15138, (30 December 1987).

N. F. Ness, M. H. Acuña, K. W. Behannon, L. F. Burlaga, J. E. P. Connerney, R. P. Lepping, and F. M. Neubauer, "Magnetic Fields at Uranus," *Science* **233**, 85–89, (4 July 1986).

F. M. Neubauer, "Nonlinear Standing Alfvén Wave Current System at Io: Theory," *Journal of Geophysical Research* **85**, 1171–1178, (1 March 1980).

E. C. Stone and E. D. Miner, "The Voyager 2 Encounter with the Uranian System," *Science* **233**, 39–43, (4 July 1986).

C. S. Wu and L. C. Lee, "A Theory of the Terrestrial Kilometric Radiation," *Astrophysical Journal* **230**, 621–626, (1 June 1979).